DOKUZ EYLÜL UNIVERSITY
GRADUATE SCHOOL OF NATURAL AND APPLIED SCIENCES

THE INVESTIGATION OF KINETICS OF LEACHING PARAMETERS OF RARE EARTH ELEMENT CONTAINING RAW MATERIALS

by
Hüseyin Eren OBUZ

November, 2020
İZMİR

THE INVESTIGATION OF KINETICS OF LEACHING PARAMETERS OF RARE EARTH ELEMENT CONTAINING RAW MATERIALS

A Thesis Submitted to the
Graduate School of Natural and Applied Sciences of Dokuz Eylül University
In Partial Fulfillment of the Requirements for the Degree of Master of Science
in Metallurgical and Materials Engineering

by
Hüseyin Eren OBUZ

November, 2020
İZMİR

M.Sc. THESIS EXAMINATION RESULT FORM

We have read the thesis entitled **"THE INVESTIGATION OF KINETICS OF LEACHING PARAMETERS OF RARE EARTH ELEMENT CONTAINING RAW MATERIALS"** completed by **HÜSEYİN EREN OBUZ** under the supervision of **ASST. PROF. MURAT ALKAN,** and we certify that in our opinion, it is fully adequate, in scope and quality, as a thesis for the degree of Master of Science

Asst. Prof. Dr. Murat ALKAN

Supervisor

Assoc. Prof. Dr. Aylin ZİYLAN

Jury Member

Asst. Prof. Dr. Mehmet Şeref SÖNMEZ

Jury Member

Prof. Dr. Özgür ÖZÇELİK

Director

Graduate School of Natural and Applied Sciences

ACKNOWLEDGMENTS

First of all, I would like to thank you, Asst. Prof. Murat ALKAN, for his support, friendship, and advice throughout my life and my graduate studies. I would like to thank Assoc. Prof. Aylin ZİYLAN and Asst. Prof. Mehmet Şeref SÖNMEZ for suggestions during the thesis examination.

I would like to thank my colleague Haydar GÜNEŞ, who has always been with me from my undergraduate, graduate, and business life and supported me in all matters.

I would like to thanks all helpful chemists, engineers and, executives in the General Directorate of Mineral Research and Exploration.

TÜBİTAK has supported this thesis in the scope of the 3501 Career Development Program with the project no 177M202.

I would like to thank the research assistant Ahmet Çağrı KILINÇ and Serhat KÖKTAŞ for their help and guidance during laboratory studies. Also, I thank Emre ÖZCAN for being a good friend and supporting me in experimental studies and my thesis writing. I present to my thanks to all of my professors that give a good background during my undergraduate and graduate periods.

I would like to special thanks to my mother, Şengül CANSEVEN, and other family members for all of their trust and support. I thank you Gamze GÜZLE for supporting to me and sharing life with me. I would like to thank you, my friend, and my brother Aşkın HAYDAROĞLU for supporting each other by growing up together since our childhood. And also, I would like to thank you, my friend, Remzi GÖMEK, for the kind and helpful.

Hüseyin Eren OBUZ

THE INVESTIGATION OF KINETICS OF LEACHING PARAMETERS OF RARE EARTH ELEMENT CONTAINING RAW MATERIALS

ABSTRACT

In this study, the leaching kinetics of Wigu Carbonite Complex ore contains rare earth elements in different acid solutions were investigated. In the experiments, two different acid solutions were used to prepare the solvent medium with the complex ore from Wigu Hill as a raw material. The leaching of ore in a solution may include multiple steps such as reaction and diffusion. The characteristics of the raw materials and reaction type are effective in determining the leaching mechanism. The shrinking core model was selected for the determination of leaching kinetics considering raw materials and reaction types. Although the shrinking core model contains five steps in itself, when these steps are formulated, only two steps are important for the determination of leaching kinetics. These two steps are classified as chemical reactions and diffusion through a product layer. Linear regression analysis, which is one of the least-squares regression methods, was performed to find the reaction rates. As a result of the linear regression analysis, determination coefficients were also calculated. The activation energy, which is another method used to determine the reaction mechanism, has been calculated. The Arrhenius equation was used to calculate the activation energy. The calculations of the activation energies were made for both two steps (chemical reaction and diffusion) by using hydrochloric and nitric acid solutions. The activation energies were calculated according to these two steps approaches. According to the results, the leaching mechanism of both cerium, lanthanum, neodymium, and praseodymium in the complex ores were mixed controlled under the selected conditions.

Keywords: Leaching, kinetics, shrinking core model, rare earth elements

NADİR TOPRAK ELEMENTLERİ İÇEREN HAMMADDELERİN ÇÖZÜMLENDİRME İLE DEĞERLENDİRİLME KİNETİĞİNİN İNCELENMESİ

ÖZ

Bu tez çalışmasında, nadir toprak elementlerini içeren Wigu Karbonitte Kompleks cevherin farklı asit çözeltilerinde çözünme kinetiği araştırılmıştır. Deneylerde çözücü ortamın hazırlanmasında iki farklı asit çözeltisi ve hammadde olarak Wigu Tepesinden temin edilen Wigu Karbonitte Kompleks cevheri kullanılmıştır. Bir malzemenin çözücü bir ortamdaki çözünme davranışı birden fazla adım içermektedir: çözücü ile çözünecek malzemenin reaksiyona girmesi ya da çözücünün çözülecek malzemeye olan difüzyonu gibi. Çözünme kinetiğinin belirlenmesinde farklı yöntemler kullanılmaktadır. Yöntemin seçilmesinde hammaddenin yapısı ve reaksiyonun türü etkilidir. Hammadde ve reaksiyon türü göz önünde bulundurulduğunda, bu çalışmada çözünme kinetiğinin belirlenmesinde yöntem olarak küçülen çekirdek modeli kullanılmıştır. Küçülen çekirdek modeli kendi içinde beş adım içermesine rağmen çözünme kinetiğinin belirlenmesinde iki adım etkilidir. Bu iki adım sırasıyla kimyasal reaksiyon ve bir ürün tabakası üzerinde difüzyon olarak sınıflandırılmıştır. Çözünme deneyi analiz sonuçları her iki adımı tanımlayan formüllerde kullanılmış ve çözünme hızı hesapları yapılmıştır. En küçük kareler regresyonu yönteminden olan doğrusal regresyon analizi yöntemi ile reaksiyon hızları elde edilmiştir. Doğrusal regresyon analizi ile ayrıca determinasyon katsayıları da hesaplanmıştır. Reaksiyon mekanizmasının belirlenmesinde kullanılan diğer bir yöntem olan aktivasyon enerjisinin hesaplanması da ayrıca gerçekleştirilmiştir. Aktivasyon enerjisinin hesaplanmasında, Arrhenius denklemi kullanılmıştır. Kimyasal reaksiyon ve difüzyon kontrollü yaklaşımlar için ölçülen aktivasyon enerjisi değerlerine bakıldığında, seçilen koşullarda kompleks cevher içindeki Ce, La, Nd ve Pr'nin çözünme süreci karışık kontrollü olarak bulunmuştur.

Anahtar Kelimeler: Liç, kinetik, küçülen tanecik modeli, nadir toprak elementleri

CONTENTS

Page

LIST OF FIGURES

Page

LIST OF TABLES

Page

CHAPTER ONE

INTRODUCTION

The rare earth elements (REEs) are a group of elements include 17 chemically similar metallic elements. Generally, REEs are divided into two subgroups, light rare earth elements (LREEs) and heavy rare earth elements (HREEs) (A. R. Jha, 2014; Krishnamurthy & Gupta, 2015).

REEs have a wide range of application areas such as magnets, catalysts, batteries, metallurgical fields, etc. Over the last decades, the demand for REEs has been increasing due to technological advances like electric cars, wind turbines, fiber optic applications. Therefore, supply risk and economic importance of REEs have become higher than other elements. According to the European Commission 2017 reports, REEs have been selected as critical raw materials (Krishnamurthy & Gupta, 2015, European Commision, 2017).

REEs are found in more than 250 minerals. However, only a few of them are used as the primary production source of REEs, such as bastnasite, monazite, and xenotime. Estimated rare earth oxide (REO) reserves are 160,000,000 metric tons. Production of REEs from primary sources mainly includes three steps: physical beneficiation, then chemical beneficiation, and purifications. Chemical beneficiation is also including three steps: leaching, solvent extraction, and precipitation (Krishnamurthy & Gupta, 2015).

The most popular leaching definition is the dissolution process of the soluble ingredients containing solid materials with different kinds of solvents. The leaching is mostly used for dissolving of the valuable elements in an ore or concentrate. Every REEs has different types of dissolutions behavior. Determination of this behavior can help to find parameters that will increase the leaching efficiency. Therefore, the kinetic science is used the find the mechanism (Gupta, 2006; Havlik, 1999).

The thermodynamic science provides information about whether a reaction occurs under certain conditions or not. However, it does not provide information about the reaction mechanism. Therefore, kinetic science is used to determine the mechanism of reactions. Kinetic is a science interested in the measurement and interpretation of reaction rates. Thus, the determination and interpretation of reaction rates help to identify mechanisms. The determined mechanisms enable the decision of the efficient parameters in a production process and the design of the process (Gupta, 2006; Richardson et al.,2002).

The reaction types and particle types are the effective parameters for the determination of leaching kinetics of REEs. In chemistry, reactions are divided into two subgroups as homogeneous reactions and heterogeneous reactions. The homogeneous reactions can be described as both reactants and products have to same phases, such as the transition of water from the liquid phase to the vapor phase. The heterogeneous reaction can be described as both reactants and products have different phases, such as the production of ammonia with nitrogen and hydrogen gases. Therefore, the REEs leaching reactions are described as a heterogeneous reaction (Şeşen, 1998).

The shrinking core model was the only model for the leaching of REEs when considering the particle shapes and reaction types. Yagi and Kunii developed this model in 1955 and 1961. The shrinking core model can be described in several steps. First, the chemical reaction occurs at the surface of the particle. After that, while reaction moves into the solid part, leaving behind converted materials and product layer, which calls the “ash” layer. During the reaction, the unreacted core of materials shrinks in size. This model was used to determine the mechanism of leaching kinetics of REEs (Gbor & Jia, 2004; Levenspiel, 1999a).

The shrinking core model is used to calculate the rate constant at different leaching temperatures and leaching durations. Then, graphs are plotted according to these

calculations. The graphs were used for calculating the values of k_r, $k_{d,}$ and R^2 and activation energy (Koech, Everson, Neomagus, & Rutto, 2014; Krishnamurthy & Gupta, 2015; Lim, Ibana, & Eksteen, 2016; Safari, Arzpeyma, Rashchi, & Mostoufi, 2009).

In this thesis, Wigu Carbonatite Complex ore from Tanzania, Wigu Hill was used as a raw material in the leaching experiments. Wigu Carbonatite Complex ore contains relatively low-grade REEs against other REEs ores. The study aimed to investigate to leaching kinetics of Ce, La, Nd, and Pr, with determining the optimum parameters for leaching of Wigu Carbonatite Complex ore.

CHAPTER TWO

THEORETICAL BACKGROUND AND LITERATURE

2.1 Rare Earth Elements

According to the International Union of Pure and Applied Chemistry (IUPAC), the rare earth elements (REEs) consist of 17 chemically similar metallic elements, including scandium (21), yttrium (39), and the lanthanides (57-71) (Gupta, 2016; Evans, 2014). REEs generally are divided into two groups; light rare earth elements (LREEs) and heavy rare earth elements (HREEs). LREEs (cerium group) include the elements from lanthanum to europium, where HREEs (yttrium group) include the elements from gadolinium to lutetium, and yttrium (A Jha, 2014).

The REEs have similar physical and chemical features. It was hard to separate, so separation took almost 160 years, from 1787 to 1941. The first discovered rare earth element was cerium in 1787. After this discovery, scientists separated REEs one by one until the discovery of promethium in 1941 (Krishnamurthy & Gupta, 2015).

More than 250 minerals include REEs. However, only a few minerals (bastnasite, monazite, and xenotime) are used for mine production of REEs. REEs in minerals are generally in their oxide forms. Rare earth oxide (REO) reserves in the world were estimated at 153,099,600 metric tons (Krishnamurthy & Gupta, 2015).

Each of REEs have different application areas; for instance, neodymium is using for the production of permanent magnets, lanthanum is using for nickel-metal hydrated batteries, etc. (A Jha, 2014). REEs consumption in 2000 was almost 75,500 tons. In 2016 REEs consumption risen up to 123,100 tons. So the demands of REEs have increased rapidly due to the technological developments (Goodenough, Wall, & Merriman, 2018).

The production route of REEs if the hydrometallurgical processes selected generally has three steps; Leaching, Solvent extraction, and precipitation. The leaching step consists of dissolution of REEs in a solution, followed by solid and liquid separation by filtration. After the separation, the solvent extraction step was started. Solvent extraction purifies the solution with enrichment of desired element contents by using organics solvents. After the purification, the selected elements are precipitated by using precipitation agents. Generally, the final product of this process can be RE-oxide or RE-hydroxide, etc.

2.1.1 History of Rare Earth Elements

The rare earth elements discovery journey was started with an "unknown earth" mineral in 1751 in Sweden by A.F. Cronstedt. After the discovery of unknown earth minerals, the mineral had been investigated by Jöns Jakob Berzelius and Wilhelm Hisinger in Sweden. So they found that this mineral was an oxide form of a new element, and then they named the element "cerium" because of the asteroid Ceres (A. Jha, 2014; Krishnamurthy & Gupta, 2015). The schematic view of the history of REEs discovery is given in Figure 2.1, Figure 2.2, and Figure 2.3, respectively.

Carl Gustaf Mosander separated a new element from ceria in 1839 and called it as "lanthanum". However, it was not the pure lanthanum; there might be still new elements. After the experiments, Mosander also detected a new element. This time he called the new element as "didymium", which means twins (Anwander, 1997; Krishnamurthy & Gupta, 2015).

In 1878 Marc Delafontaine suspected that didymium was not a single element due to its absorption spectrum. Paul Emile Lecoq de Boisbaudran disproved Delafontaine; however, he found a new element, "samarium" in samarskite. Carl Auer von Welsbach suspected that didymium might now a single element. Welsbach succeeded to the separation of didymium into two elements, which were "praseodymium" and "neodymium" (Krishnamurthy & Gupta, 2015).

Carl Axel Arrhenius discovered a gadolinite mineral, but he did not say anything to anyone (1787). After that, Johan Gadolin analyzed this mineral in 1794. Gadolin realized that this mineral contains silica, iron, and also “new earth”. After the discovery of “new earth”, Anders Gustaf Ekeberg confirmed his discovery. Gadolin gave the name of this mineral “gadolinite”, but also, Ekeberg gave another name, which was “yttria” (Anwander, 1997; Krishnamurthy & Gupta, 2015).

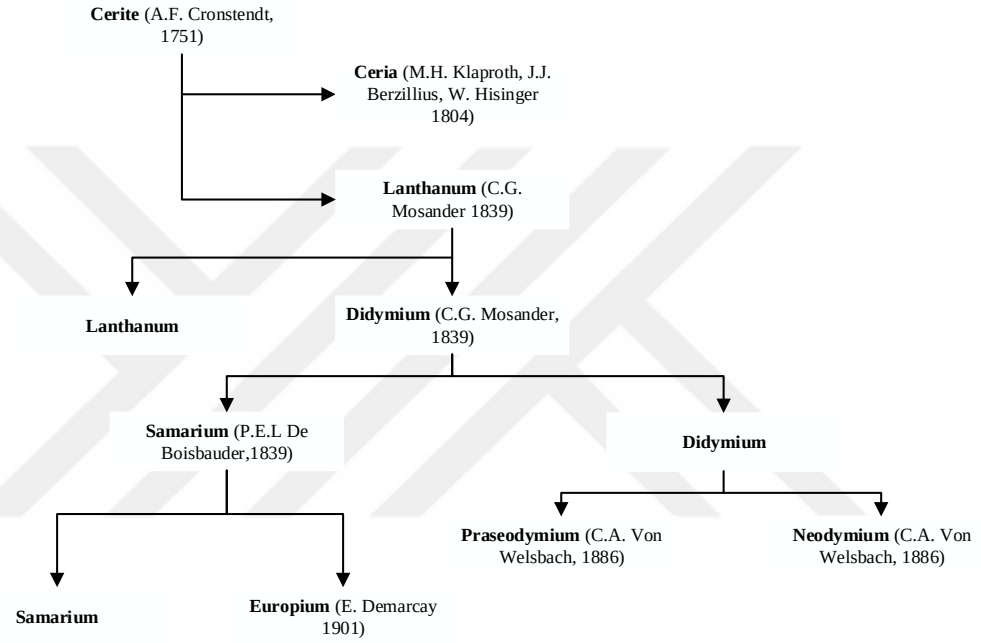

Figure 2.1 Discovery of REEs over the years part 1 (Krishnamurthy & Gupta, 2015)

The word "Earths" was accepted as an element until Antal Ruprecht. Ruprecht realized that these were compound instead of elements. However, this discovery was confirmed by Sir Humphrey Davy. At the beginning of the nineteenth century, chemists did not produce yttrium in pure. However, they began to call yttrium instead of yttria (Anwander, 1997; Krishnamurthy & Gupta, 2015).

Subsequently, Mosandar noticed that gadolinite includes yttrium, and then reported that gadolinite included two more elements, which were “erbium” and “terbium”. Beginning of the 1850s, Marc Delafontaine proved that the yttrium, erbium, and terbium were different elements. He also changed the names erbium to terbium and

terbium to erbium in 1864. In 1864, Jean Charles Marignac found a new element in gadolinite, and he named as “ytterbium”. Marignac gave this report Lars Frederic Nilson for the confirmation of "ytterbium”. Lars Frederic Nilson confirmed the existence of ytterbium. Besides, Nilson dissolved gadolinite in nitric acid, and the solution yielded a weak absorption line in the red and the green spectrum. Nilson considered that this could be a new element and gave it a name as “scandium” in 1879 (Anwander, 1997; Krishnamurthy & Gupta, 2015).

After the separation of ytterbium from erbium, Per Theodor Cleve investigated erbium fraction to find a new element. Cleve realized that after the chemical separation and analysis, there were two new elements existences. He called them as “thulium” and “holmium” in 1879 (Krishnamurthy & Gupta, 2015).

In 1886, Boisbaudran had investigated gadolinite again by using different chemical separation methods and different analysis techniques. Consequently, Boisbaudran identified that holmium had contained another fraction and he named it as “dysprosium” (Krishnamurthy & Gupta, 2015).

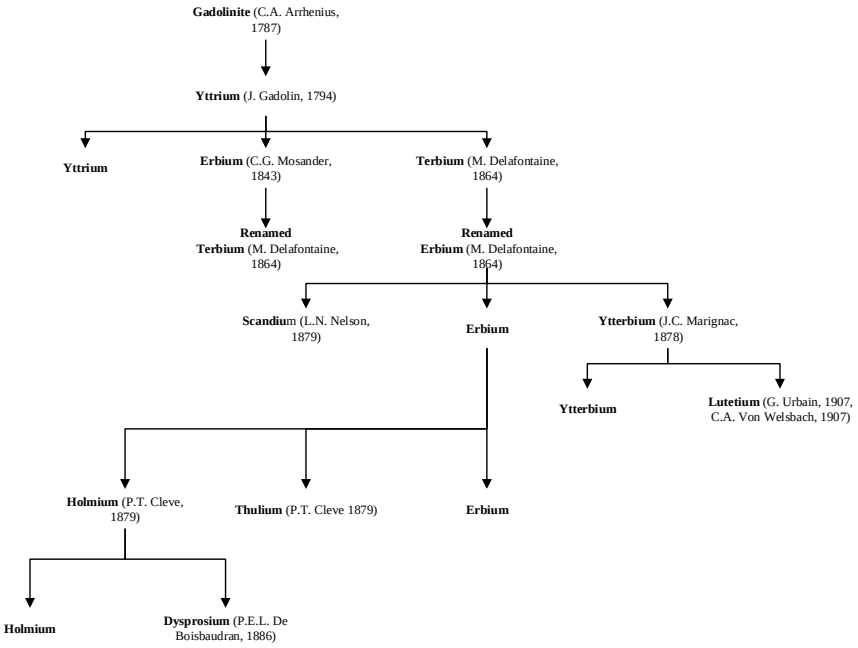

Figure 2.2 Discovery of REEs over part 2 (Krishnamurthy & Gupta, 2015)

After Boisbaudran discovered samarium, Eugene Demarcay announced a new element from the samarium after 15 years (1901). He named it “europium”. In 1904, europium was also separated from gadolinium. In 1905, Georges Urbain found that ytterbium consisting of two more elements, “neoytterbium” and “lutetium” (Krishnamurthy & Gupta, 2015).

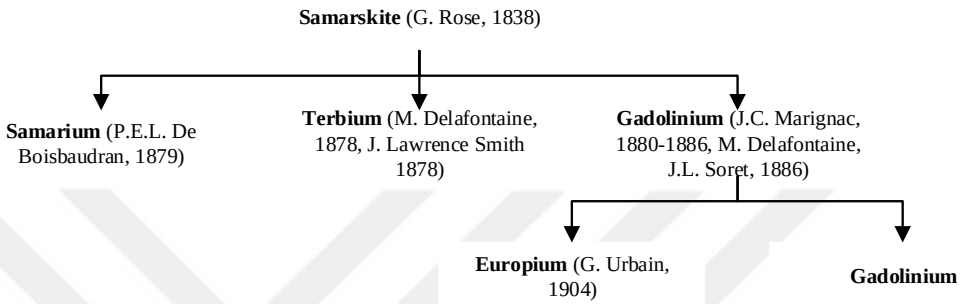

Figure 2.3 Discovery of REEs over part 3 (Krishnamurthy & Gupta, 2015)

2.1.2 Special Characteristic of Rare Earth Elements

Because of the similar properties of REEs, scientists had worked for 160 years on the separation of REEs from each other. Generally, REEs are found together in the same ores, so this situation also creates a big deal for separation from each other. Experimental studies prove that REEs and their compounds have similar chemical properties consequence of similar electron configuration (Krishnamurthy & Gupta, 2015).

2.1.2.1 Electron configuration

Electron configuration is directly related to the chemical behavior of atoms. In the atom, the electron shells can be represented like; K, L, M, N, O, P, and Q or 1, 2, 3, 4, 5, 6, and 7. K is the first shell and Q is the last. Moreover, every electron shells have subshells; the electron subshells can be described as; s, p, d, and f orbitals. Every subshell contains a limited number of electrons. For example, s subshell is filled in 2 electrons, where p needs 6 electrons for filling. The electrons filling in subshells

depend on The Madelung's Rule and it can be represented in Fig. 2.4. (Krishnamurthy & Gupta, 2015).

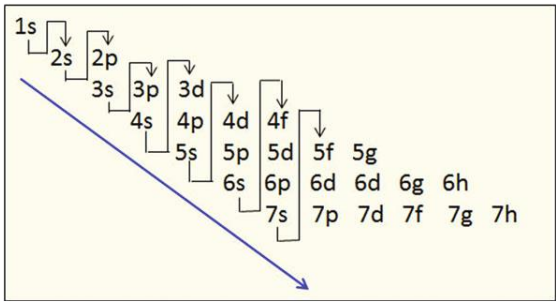

Figure 2.4 Description of the Madelung Rule (Krishnamurthy & Gupta, 2015)

The electron configurations of scandium, yttrium, and lanthanum were a successive series of transition elements. The valance electron configurations of scandium, yttrium, and lanthanum were formulated as; $ns^2\ (n\text{-}1)\ d^1$ where *n= 4, 5, and 6,* respectively. So scandium, yttrium, and lanthanum have no electrons in *f* orbital. The other 14 elements starting from cerium to lutetium have valence electron configuration formulated as; $6s^2 5d^1 f^{n-1}$ or $6s^2 4f^n$. The REEs oxidation possibilities were given in Table 2.1 (Krishnamurthy & Gupta, 2015).

Table 2.1 Electron Configuration and oxidation possibilities of REEs (Krishnamurthy & Gupta, 2015; Zhang, Zhao, & Schreiner, 2016)

Element	Atom	M^{2+}	M^{3+}	M^{4+}	Element	Atom	M^{2+}	M^{3+}	M^{4+}
La	$5d6s^2$	$5d$	[Xe]	-	**Tb**	$4f^9 6s^2$	$4f^9$	$4f^8$	$4f^7$
Ce	$4f^1 5d^1 6s^2$	$4f^2$	$4f$	[Xe]	**Dy**	$4f^{10} 6s^2$	$4f^{10}$	$4f^9$	$4f^8$
Pr	$4f^3 6s^2$	$4f^3$	$4f^2$	$4f$	**Ho**	$4f^{11} 6s^2$	$4f^{11}$	$4f^{10}$	-
Nd	$4f^4 6s^2$	$4f^4$	$4f^3$	$4f^2$	**Er**	$4f^{12} 6s^2$	$4f^{12}$	$4f^{11}$	-
Pm	$4f^5 6s^2$	-	$4f^4$	-	**Tm**	$4f^{13} 6s^2$	$4f^{13}$	$4f^{12}$	-
Sm	$4f^6 6s^2$	$4f^6$	$4f^5$	-	**Yb**	$4f^{14} 6s^2$	$4f^{14}$	$4f^{13}$	-
Eu	$4f^7 6s^2$	$4f^7$	$4f^6$	-	**Lu**	$4f^{14} 5d6s^2$	-	$4f^{14}$	-
Gd	$5f^7 5d6s^2$	$4f^7 5d$	$4f^7$	-	**Sc**	$[Ar]3d4s^2$	-	[Ar]	-
Y	$[Kr]5d^1 6s^2$	-	[Kr]	-					

The oxidation stages of REEs can be in the form of M^{2+}, M^{3+}, and M^{4+} ions. In the M^{3+} ion form, scandium, yttrium, and lanthanum have an inert gas configuration. The electron configuration of f^0, f^7, and f^{14} are used to determine the oxidation state of +2 and +4 of REEs ion forms. The electron configuration gives important information for determining the existence of oxidation states for the REEs. However, thermodynamic and kinetic factors also affect the stability of oxidation states of REEs. Thus, all factors should be examined in determining the oxidation state of REEs (Krishnamurthy & Gupta, 2015; Zhang et al., 2016).

2.1.2.2 Lanthanide Contraction

Lanthanide contraction describes that when the atomic numbers of REEs were increasing, the ionic radius regularly decreased. The reason is that the atomic radius shielded by directional *4f* electrons, and every increases in the atomic number results *4f* orbitals to gain another electron. Thus, lanthanum has the largest and the lutetium has the smallest ionic radius. As a result, the contraction was directly affected by *4f* orbitals (Krishnamurthy & Gupta, 2015; atMcLennan & Taylor, 2012; Voncken, 2015; Atwood, 2013). Figure 2.5 represents the lanthanide contraction.

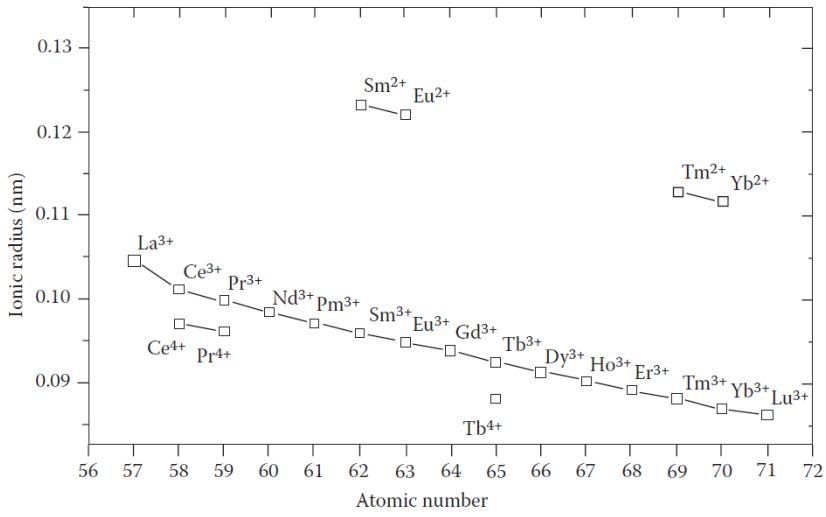

Figure 2.5 The relationships between the ionic radiuses to atomic number for REEs (Krishnamurthy & Gupta, 2015)

As a result of the lanthanide contraction, yttrium has an ionic radius comparable to that of the heavier REEs species in the holmium-erbium region (Voncken, 2015). Also, yttrium chemically processes with HREEs. Though, it is difficult to separate from the HREEs. Besides this, scandium has a much smaller atomic radius, and M^{+3} ionic size is much smaller than the HRREs. For these reasons, scandium generally does not occur with rare earth minerals. Moreover, scandium chemical properties are considerably different from the other REEs (Krishnamurthy & Gupta, 2015).

Another consequence of Lanthanide contraction is that REEs can replace each other in the same crystal structure. This situation made it difficult to separate REEs from each other. On the other hand, this situation also REEs provides separation with solvent extraction and ion exchange methods (Krishnamurthy & Gupta, 2015; McLennan & Taylor, 2012; Voncken, 2015; Atwood, 2013).

2.1.3 Demands and Usage Areas of Rare Earth Elements

Since the discovery and extraction of REEs, the uses of them have increased day by day. Today, REEs are needed to make progress in the technological field and they are using in many different technological fields. REEs are using in advanced electronic devices (such as nickel metal hydrate batteries, permanent magnets, etc.), power generators (such as wind turbine generator system, etc.) and military applications. As the results of this demand, REEs production has increased rapidly. The usage area of REEs is represented in Figure 2.6 (Goodenough et al., 2018; Humphries, 2013; Rollat, Guyonnet, Planchon, & Tuduri, 2016).

In 2000, the global REEs demand was 136,100 tons. In line with rising demand, global REEs market increased to 210,000 tons in 2015. In the technology developed, REEs usage areas have integrated into new areas such as electronic cars, NdFeB hard magnets, glass fibers for fiber optic application to improve data transfer feeds, etc. (Goodenough et al., 2018).

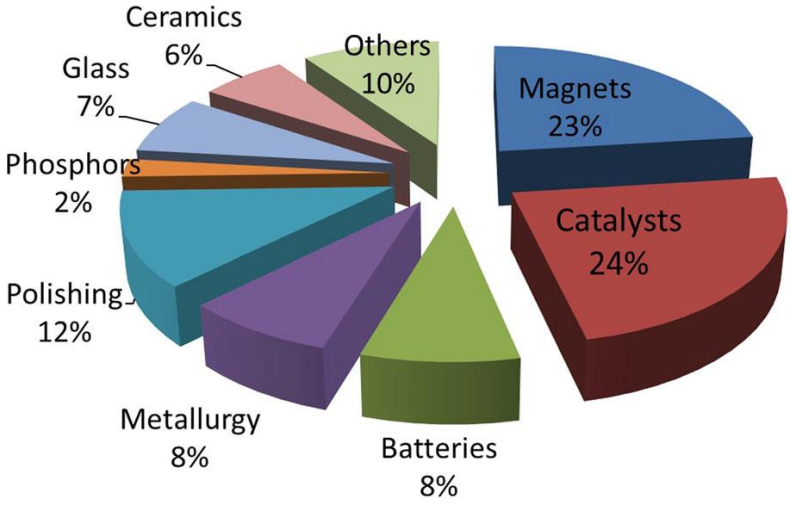

Figure 2.6 Current usage areas of REEs (Goodenough et al., 2018)

According to Rollant (2016), the global demand for REEs in 2014 was 118,000 tons, while their supply was 143,000 tons (Figure 2.7). When 2020, Rollant estimated that the demand would raise to 170,000 tons (Goodenough et al., 2018). Technological developments could explain this increase. For instance, NdFeB demand has increased rapidly because of the wind turbine and hard magnets production. Furthermore, Ni-MH batteries production has increased because of hybrid cars (Goodenough et al., 2018; Rollat et al., 2016).

According to European Commission report (2017), REEs have been selected as critical raw materials because of their supply risk and economic importance. As seen in Fig 2.8, LREEs and HREEs have the highest supply risk and middle economic importance, depending on 2017 repots. (European Comission, 2017) . So for all of these reasons, REEs supply risk and economic importance would be raised in the next decade, and also their demand would be raised.

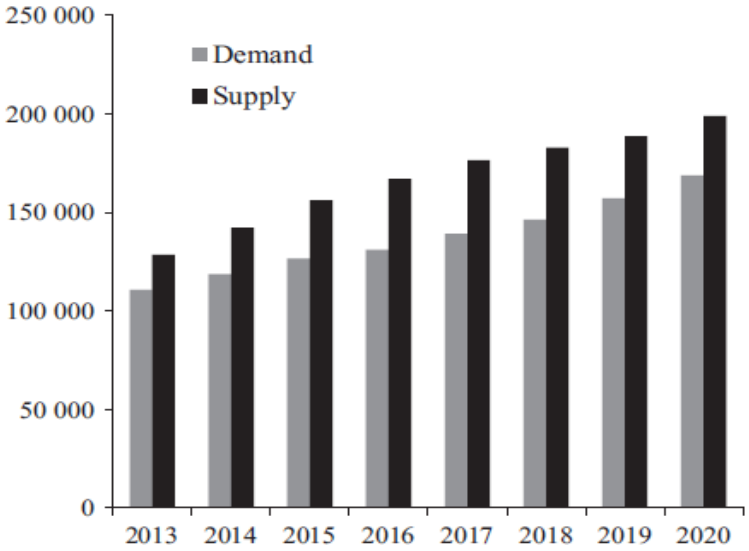

Figure 2.7 Estimated global REEs supply and demand (Rollat et al., 2016)

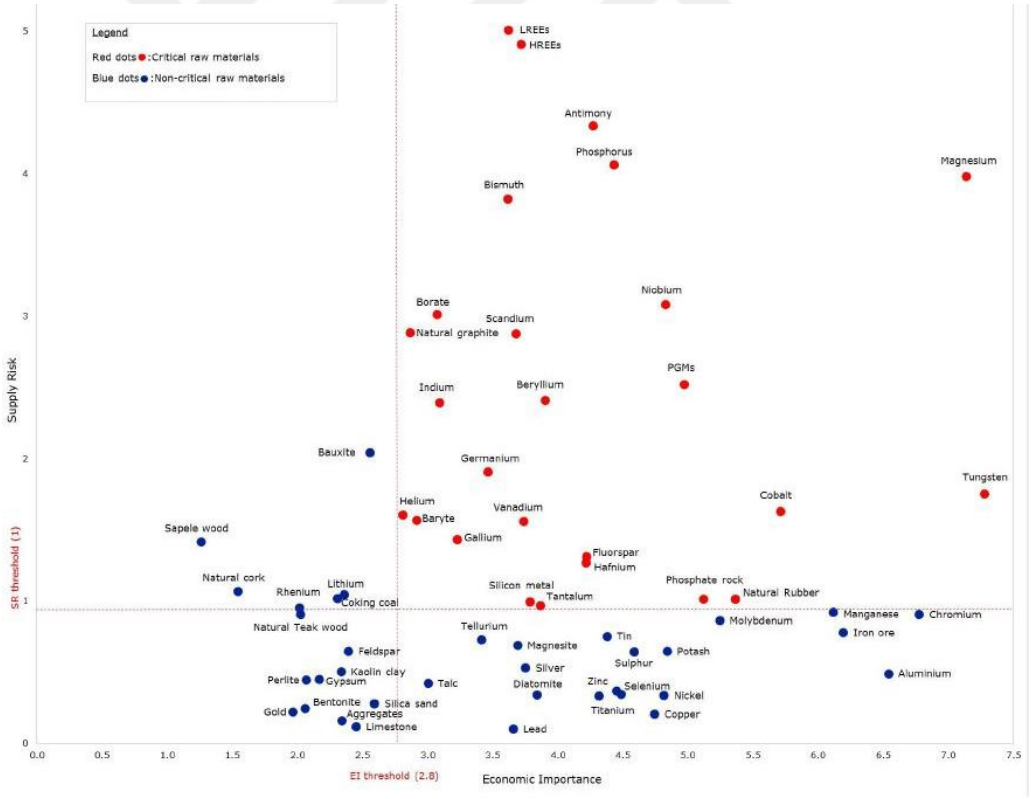

Figure 2.8 Supply risks and economic importance of materials and critical raw materials stated by European Commission (European Comission, 2017)

2.1.4 Primary Sources of REEs

In nature, REEs are not found in the element state, and also, they are not found as individually. Generally, 160 different kinds of minerals include REEs; however, only a few of them suitable for the production of REEs. REEs have strong affinity for oxygen, so REEs are found mostly in oxidic compounds in nature such as oxides, phosphates, carbonates, and silicates (Krishnamurthy & Gupta, 2015; Qi, 2018). At present, three different minerals are used for the production of REEs as primary sources. These minerals are monazite, bastnasite, and xenotime. The content of minerals was given in Table 2.2 (Krishnamurthy & Gupta, 2015; Voncken, 2015).

Table 2.2 Chemical formula and contents of REEs in Minerals (Krishnamurthy & Gupta, 2015)

Minerals	Formula	Contents (wt. %)		
		REO	ThO_2	UO_2
Monazite (Ce)	(Ce, La, Nd, Th)PO_4	35-71	0-20	0-16
Bastnasite (Ce)	(Ce, La)$(CO_3)F$	70-74	0-0.3	0.09
Xenotime	YPO_4	52-67	0-5	0-5

REEs reserves and production represented in Table 2.3. The leader of REEs mine production is China. Chine mine production was 105,000 metric tons in 2016 and 2017. Moreover, China also has the highest REEs reserves in the World. After China, Australia is the second in the mine production. However, the second-highest REEs reserves, which is 22,000,000 metric tons, is found in Brazil (Gamboghi, 2019).

REEs World production, reserves, and U.S. imports were represented in Figure 2.9 for 2011. In 2011, China produced 95% of the Worlds REEs. China exported 31,438 metric tons of REEs to U.S. for 2011 and 2012 (Humphries, 2013). China exported 39,800 mt of REEs compound in 2017, which was higher than in 2016. Australia's REEs production were done in Malaysia by using Australia's domestic ores. In 2016, Malaysia increased its REE exports by 57% in 2017 (Gamboghi, 2019).

Table 2.3 World production and reserves for REEs (Gamboghi, 2019)

Country	Mine production (Metric tons) 2016	2017	Reserves (Metric tons)
United States	-	-	1,400,000
Australia	15,000	20,000	3,400,000
Brazil	2,200	2,000	22,000,000
Canada	-	-	830,000
China	105,000	105,000	44,000,000
Greenland	-	-	1,500,000
India	1,500	1,500	6,900,000
Malawi	-	-	140,000
Malaysia	300	300	30,000
Russia	2,800	3,000	18,000,000
South Africa	-	-	860,000
Thailand	1,600	1,600	NA
Vietnam	220	100	22,000,000
World Total	129,000	130,000	120,000,000

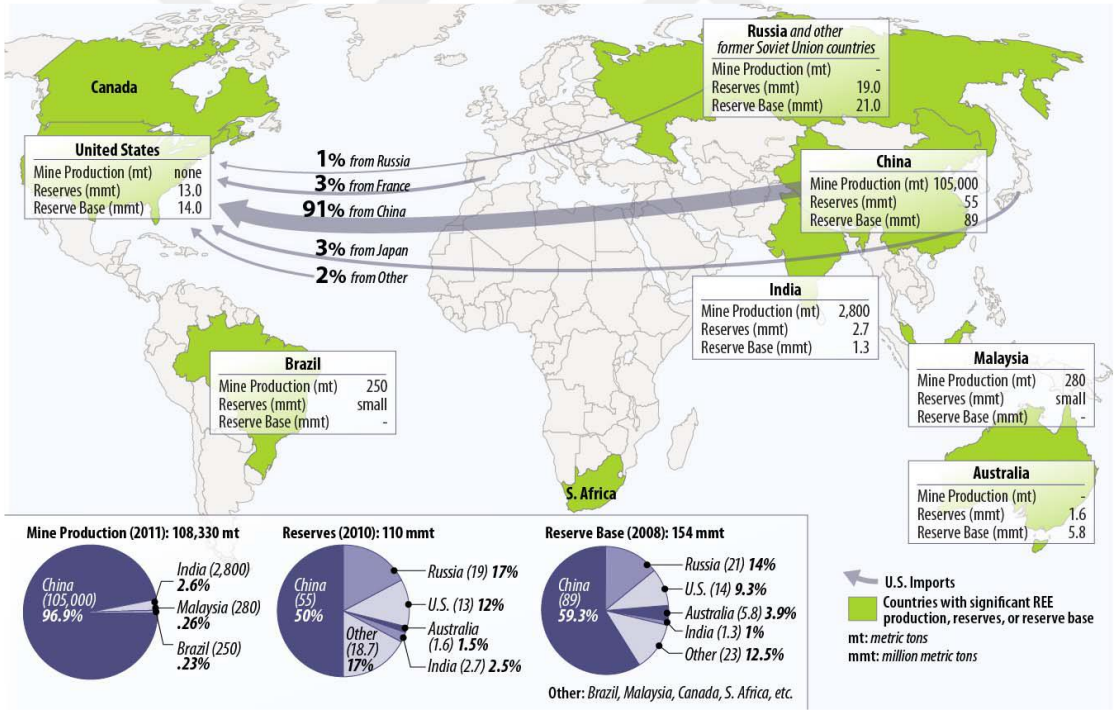

Figure 2.9 Rare earth elements World production, reserves and U.S. imports (Humphries, 2013)

2.1.4.1 Monazite

Monazite comes from the Greek word monazeis, means “to be alone”. This meaning comes from the isolated crystals of monazite and also, the mineral was rare when it was first discovered (Voncken, 2015). The mineral monazite includes the cerium group (Ce, La, Y) and thorium. The monazite is a phosphate mineral, so the general formula is (Ce, La, Nd, Th)PO_4. Monazite has a high resistance to chemical weathering. Due to chemical resistance and high specific gravity (4.8 to 5.5 g/cm^3), monazite is accompanied by other heavy minerals such as ilmenite, magnetite, rutile, and zircon in deposits. Monazite mineral colors are yellow to brown or orange-brown colors (Figure 2.10) (Krishnamurthy & Gupta, 2015).

Figure 2.10 Monazite mineral found in Iveland Satesdal, Norway (Voncken, 2015)

Acidic igneous rocks and metamorphic rocks may include monazite as an accessory mineral. The primary monazite deposits have been found in Van Rhynsdorp and Naboomspruit (South Africa), in Colorado (United States), and in Bayan Obo (China). The most critical monazite resources are beach sand deposits, including other heavy minerals like ilmenite, rutile, and zircon. Monazite contains about 70% REO and the mass fraction of REEs is 20-30% Ce_2O_3, 10-40% La_2O_3; also includes a significant amount of neodymium, praseodymium, samarium, and a lesser amount of dysprosium, erbium, and holmium. Besides, some thorium contents of 4-12 mass% are common (Krishnamurthy & Gupta, 2015).

2.1.4.2 Bastnasite

Swedish chemist Wilhelm Hisinger discovered Bastnasite in 1838. Bastnasite includes LREEs like Monazite; however, it also contains one HREEs: Y(Voncken, 2015). Bastnasite does not contain U or Th. Bastnasite (Ce, La, Y)CO_3F has a similarity to other minerals such as hydroxyl-bastnasite (Ce, La)CO_3(OH, F) and parasite Ca(Ce, La)$_2$(CO_3)$_3F_2$. Bastnasite mineral are pale white, tan, gray, brown, yellow, or pink color (Figure 2.11) (Krishnamurthy & Gupta, 2015; Voncken, 2015).

Figure 2.11 Bastnasite mineral found in, Mountain Pass California (Krishnamurthy & Gupta, 2015; Voncken, 2015)

Bastnasite minerals may occur with different minerals. For example For example, in California Bastnasite complex mineral includes carbonate-silicate rocks with alkaline. In Burundi, Bastnasite occurs in quartz veins that cut micaceous schist and quartzite. In other words, even if the structures of the minerals are the same, their form of formation can be different. Bastnasite contains about 70 mass% of REO and mostly LREEs. The primary source of bastnasite deposit is Bayan Obo located in China (Krishnamurthy & Gupta, 2015; Voncken, 2015).

2.1.4.3 Xenotime

Berzelius was the first discovered xenotime in 1825. The name comes from Greek words Xenos means “foreign” and time means “honor”. The chemical formula is YPO_4. Xenotime, on the contrary to Bastnasite and monazite, contains Y and HREEs. Xenotime may include up to 67 mass % of REO. Xenotime can be yellowish-brown

to reddish-brown, occasionally gray, salmon pink, and green in color (Figure 2.12). Xenotime can easily be confused with zircon owing to a similar crystal structure (Krishnamurthy & Gupta, 2015; Voncken, 2015).

Figure 2.12 Xenotime mineral located in Madagascar (Voncken, 2015)

Xenotime may include monazite 0.5-5 mass%. Xenotime minerals are located in Malaysia, in Australian, in Indonesia, Thailand, and China.

2.1.5 Production of Rare Earth Elements from Primary Sources

The production of REEs from primary source (ores) generally starts with physical beneficiation such as grinding or crushing. After physical beneficiation, chemical beneficiation involving hydrometallurgical operations is followed. Usually, the hydrometallurgical technique includes three steps; leaching, solvent extraction, and precipitation (Krishnamurthy & Gupta, 2015).

The leaching process is the separation of the compounds turn into anions or cations in the solutions by using various chemicals. The method was the firstly used for gold production and now it has been used for a lot of elements (William D Callister Jr, 2013). The leaching process is applied into ores or concentrates, which include valuable minerals. Moreover, it is also applied into secondary sources containing valuable minerals. Furthermore, it's also used to remove impurities from concentration for beneficiation of concentration (Gupta, 2006).

The solvent extraction method can be defined as a separation method based on mass transfer between two immiscible liquid phases. These phases are called aqueous phase and organic phase. This method involves two basic steps as loading and stripping, but if it is necessary, a washing step is also included between two steps (Zhang et al., 2016).

The precipitation process is accomplished by adding a reagent such as oxides, hydrated oxides, hydroxides, or hydrated salts for precipitation of compounds. This method used for precipitation of valuable elements from aqueous solutions and also removing of impurities (Gupta, 2006).

2.2 Leaching Concept

The most common definition of the Leaching process is the process of dissolving a solid material with the help of a solvent. The leaching process is used for dissolving valuable elements in the ores or concentrates. The term leaching is also used for the dissolution process of secondary sources. Out of special situations, leaching is also applied to remove impurities in the concentration for increasing the purity of concentration. The best description is the hydrometallurgical beneficiation (Gupta, 2006; Havlik, 1999).

The leaching concept can be considered in three stages: the phase changing of solute material during leaching, the diffusion of the solvent in the pores of the solid particle, the transferring of the dissolvent particle from the solution. Any of these stages can be responsible for the limiting of dissolution behavior (Richardson et al., 2002).

The thermodynamic and kinetic approach are vital for the determination of the hydrometallurgical process. The thermodynamic approach provides a basic guidance for the selection of reagents by taking advantage of free energy changing. The kinetic considerations are much more critical than thermodynamics in the hydrometallurgical process. The hydrometallurgical process occurs relatively low temperatures than the

pyrometallurgical process. Therefore, the reaction rate of hydrometallurgical process is lower than the pyrometallurgical process. The kinetic approach can be used to determine the slowest steps. Thus, reaction rates can be increased by finding the slowest step. For these reasons, kinetic consideration is gaining much more importance than thermodynamic (Gupta, 2006; Richardson et al., 2002).

2.3. Kinetic of Metallurgical Process

The probability of metallurgical process, transformation, chemical change, regardless of the path and duration are determined by the science of thermodynamics (Şeşen, 1998). Thereby, thermodynamics does not give any information about the mechanism steps of chemical reactions and any indication of the rate at when the equilibrium would be reached. However, kinetic science investigates the chemical reaction mechanism and the reaction rates (Ray, H. S., & Ray, S., 2018; Vignes, 2013).

Kinetic science is defined as the branch of science that studies the effects of chemical reactions, and the mechanisms and speeds of change and/or transformation with the help of substance and energy properties. Kinetic science makes it possible to identify the parts that cannot be determined by the science of thermodynamics. Thus, methods and design criteria related to change or transformation can be determined. If the mechanism of processes can be revealed, the possibility of interfering with change or transformation may arise (Bokstein, Mendelv, & Srolovtz, 2005; Şeşen,1998).

Kinetic science not only researches the measurements, but also interprets these measurements. Kinetic provides quantitative information to understand the chemical reactions behind theories. Thus, measurements and interpretation of reaction rates assist for designing a process and also help to understand the mechanism (Ray, H. S., & Ray, S., 2018).

The mass transport type, temperatures, addition of a catalyst**,** particle type and reaction types are the main factors in kinetic science. Each of these factors has an effect

on the reaction rate. At the same time, these factors are also directly influential to the determination the kinetic model. Thus, every parameters should be investigated for the selection of the model (Şeşen, 1998).

2.3.1 Reaction Types

In kinetic science, reactions are divided into two subgroups as homogeneous and heterogeneous reactions. If the reactants and products in a reaction are in the same phases, the reaction is called homogeneous reactions. If the reactants and products are in different phases, the reaction is called a heterogeneous reaction. In other words, if the reaction takes place in one phase alone is called homogeneous reaction; otherwise, the reaction takes place in two or more phase is called heterogeneous reactions (Bokstein et al., 2005). A good examples of homogeneous reaction is the neutralization of an acid by a base in an aqueous medium ($H^+ + OH^- = H_2O$) and also another example is solid-state metallurgy in lattice diffusion. A good examples of heterogeneous reactions are; the reaction of metals with acids, the electrochemical changes that occur in batteries and electrolytic cells and corrosion (Gupta, 2006). However, some reactions do not occur in one step, and it may involve more than one step. The slowest steps of these reactions is considered as the controlling mechanism of the reaction (Şeşen, 1998).

In some processes, the reaction seems to be a heterogeneous reaction but, in fact, it takes place as a homogeneous reaction. For example, the oxidation of Fe^{+2} ion with oxygen involves two phases, however this process is essentially a homogeneous reaction. Since the oxygen transformation rate from the gas phase to the aqueous solution is faster than the oxidation rate of the Fe^{+2} ion, the oxidation of the Fe^{+2} ion occurs in the aqueous solution phase. So this process is a homogeneous reaction (Şeşen, 1998).

There is an important difference between the homogeneous and heterogeneous reactions in terms of the formation. Unlike the homogeneous reactions, the reactions

are occurred at the interface between the phases in heterogeneous reactions (Gupta, 2006).

The reaction type has a direct effect on determining the model of the reaction mechanism. The metallurgical transformations and reactions are mostly heterogeneous, so only the heterogeneous reaction types were investigated in this thesis.

2.3.2 Reaction Rate

A reaction rate can be defined as either the rate of production of the products or the rate of consumption of the reactants (Ray, H. S., & Ray, S., 2018). The reaction rate is generalized with a formula given Equation 2.1 (Şeşen, 1998).

$$\boldsymbol{Reaction\ rate} = \frac{\boldsymbol{Amount\ of\ transformation\ material}}{\boldsymbol{Observation\ Time}} \tag{2.1}$$

If a graph of amount of material is drawn at different durations, the slope of this curve gives the reaction rate. Besides, if the amount of the transformed material is processed according to the selected kinetic models, the completion time of the reaction can also be determined. The reaction rate can be constant, descending, or ascending speed (Şeşen, 1998).

A constant speed can only be achieved under certain conditions. These conditions are ideal; the solid surface area, entrained concentrations, and temperature remain constant throughout the process. In time, the decreasing in the reaction rate can be achieved with the reduction of the surface area of the solid is carried out by reducing the concentration of the substances and forming the product layer, which prevents the reaction on the solid surface (Şeşen, 1998).

Over time, the increased reaction rate is provided by the product (substance or energy) to improve the reaction. In such reactions, it is necessary to determine the duration for the completion of the conversion and its conditions. For the control mechanism of these reactions, concentrations, temperature, and mixing speed can be effective (Şeşen, 1998).

The controlling mechanism for each reaction is characteristic, and the slowest step is determined as the control step (Şeşen, 1998).

2.3.3 Activation Energy

The activation energy defined as the least possible amount of energy (minimum), which is required to start a reaction. The activation energy of a reaction can be influenced by a catalysts. The catalyst does not change the balance of chemical equilibrium, but it effects the reaction rates. This is due to the lowering of the energy barrier (Figure 2.13), the reaction coordinate can be any variable to define the progress along the reaction path. This could be time, the distance between reacting particles, etc. (Ray, H. S., & Ray, S., 2018).

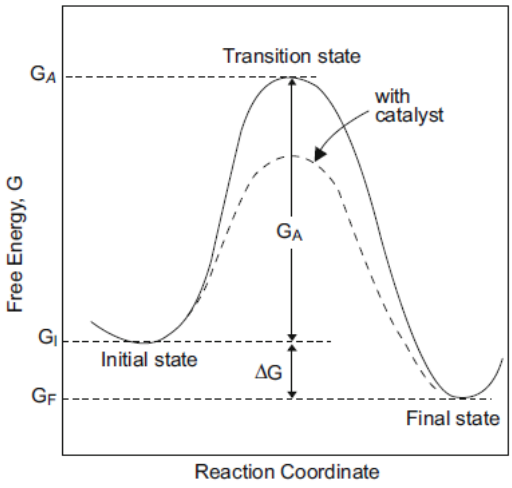

Figure 2.13 Schematic diagram showing the energy barrier and effect of catalyst. G_A is the activation of free energy (Ray, H. S., & Ray, S., 2018)

In kinetic science, the activation energy is calculated by the slope of the function between the logarithm of the rate constant (k) and the inverse of the temperature (1 / T) according to the selected model. An example is given in Figure 2.14 (Huang, Dou, Zhang, & Liu, 2017).

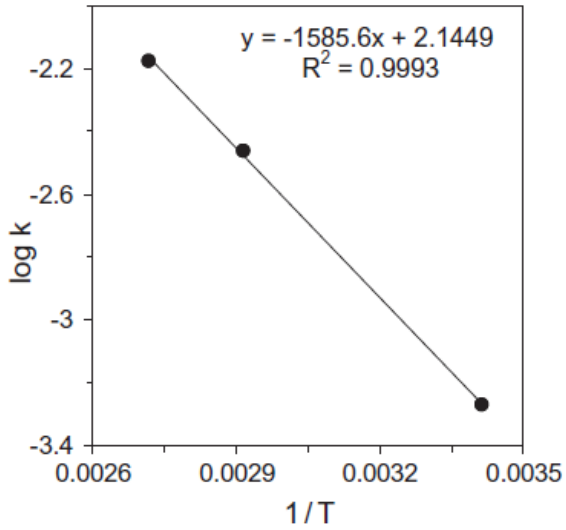

Figure 2.14 The activation energy calculations done by a study on the determination of leaching kinetics for nickel from Turkish laterite ore (Girgin, Obut, & Üçyildiz, 2011)

Today, the Arrhenius equation is also used for the calculation of the activation energy, and for the determination of reaction mechanism. The Arrhenius formula is given Equation 2.2, where *k* is the rate constant, *A* is an integration constant (frequency factor), *E* is the activation energy, *R* is the gas constant, and *T* is the absolute temperature (Huang et al., 2017).

$$\boldsymbol{k = A\, exp\,[-E/RT]} \qquad (2.2)$$

2.3.4 Reaction Degree

The degree of a reaction is the classification of a reaction rate according to conversion of the reactant concentrations. The rate of a reaction can also be defined by

a time-dependent function of the concentration of input substances. A general reaction is given in Equation 2.3 and its velocity relation in Equation 2.4.

$$aA + bB + \ \ldots \rightarrow Products \tag{2.3}$$

$$-\frac{d[A]}{dt} = k\ ([A]^a[B]^b \ldots) \tag{2.4}$$

In equation 2.5, square brackets refer to the specified ion concentrations. Negativity refers to the decreasing of raw materials over time. The sum of all (a, b, etc.) gives the degree of reaction. The degree of reaction indicates how many molecules should collide at the same time for input substances to react with each other. If the degree of a reaction is known, it is possible to use models specific to these grades for kinetic measurement. Each reaction degree has its own unique equation based on Equation 2.4. The degree of the reaction and rate constant can be calculated by using of the correlations obtained by applying certain integrals with limits of $[A_0]$ and [A] on both sides of this equation. The degree of reaction and rate constant can be calculated by the connections to be obtained in integrals of this equation with the limits of $[A_0]$ and $[A]$. The correlations of 0, 1, 2 and 3 degrees are given in Table 2.4 (Bokstein et al., 2005).

Table 2.4 Speed constant of reaction degrees and linearity in graphical method

Degree	Speed Constant	Linearity control
0	$[A] = [A_0] - kt$	$[A] - t$
1	$log[A] = -\frac{kt}{2.303} + log[A_0]$	$log[A] - t$
2	$\frac{1}{[A]} = \frac{1}{[A_0]} + kt$	$\frac{1}{[A]} - t$
3	$\frac{1}{[A]^2} = \frac{1}{[A_0]^2} + 2kt$	$\frac{1}{[A]^2} - t$

In the experimental method, the conversion rates are measured at certain durations. Then, this value is written in place for the rate constant relations for each degree and it is checked which of the resulting k values are close to each other. In the graphic method, the procedures are specified in the linearity control of Table 2.4 are applied for each certain duration. A graph is drawn for each degree, and the curve with the highest linearity determines the degree of reaction. If no distinction can be made between the linearity values, it is not possible to determine the degree of reaction (Girgin et al., 2011; Şeşen, 1998).

2.3.5 Particle Shapes

Particle shapes affect the dissolution behavior of the sample. If a solid reactant is initially nonporous, the reaction occurs at the interface between phases. If the solid reactant is initially porous, the fluid will diffuse into the solid while the reaction is occurred (Sohn, Sohn, & Wadsworth, 1979).

The conversion rate of a particle for particulate kinetics depends on size and shape (porous or non-porous) of the solid particle in an exothermic or endothermic reactions. The kinetic model should be chosen according to particle shape (porous, non-porous, or dense) (Gupta, 2006; Ray, H. S., & Ray, S., 2018; Vignes, 2013).

This kind of reaction type generally occurs in extractive metallurgy. An excellent example of reaction type is the leaching of minerals from ores or concentrates.

The shirking core model is used to explain how the leaching mechanism of REEs occurs. The shrinking core model for non-porous spherical particles is represented in Figure 2.15 (Huang, Dou, Zhang, & Liu, 2017; Kim et al., 2014; Yoon et al., 2014). The chemical reaction is occurred firstly at the outer surface of the particle. After zone of the reaction moves into the solid, completely converted materials called product layer (ash) is left. During the reaction, the unreacted core of the particle shrinks in size (Levenspiel, 1999a). This model was developed by Yagi and Kunii (1955 and 1961).

They had explained the spherical particle of unchanging size at five steps (Gbor & Jia, 2004; Levenspiel, 1999a).

The description of the shrinking core model is starting with the transferring of reactants through to the surface of the particle, then the reaction-diffusion through the blanket of ash to the surface of the unreacted core. After that, the chemical reaction is occurred at the unreacted core surface. The fourth step is the diffusion of the product through the back to the ash layer from the solid surface. The final step is the diffusion of the products through behind the liquid film layer (Levenspiel, 1999a).

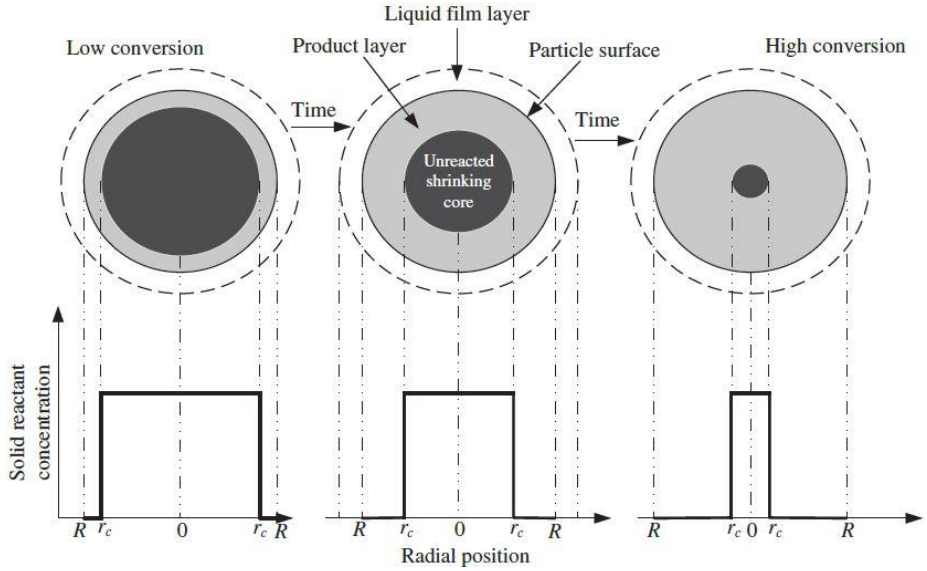

Figure 2.15 Graphical representation of the shrinking core model for unreacted core (Levenspiel, 1999a)

After the calculation of the conversion equation for spherical particle, step 1, step 2, and step 5 have the same rate equation. Thus, only two-equation remain in determining the leaching mechanism of REEs (Levenspiel, 1999a).

2.3.5.1 Diffusion through a product layer is controlling mechanism

A schematic representation of the diffusion through a product layer as the control mechanism is given in Figure 2.16. A two-step analysis should be done to develop an expression between radius and time. In the first step, the examination of a typical

partially reacted particle is done for the flux relationships at selected condition. Then, integration of r_c between R and 0 is applied for all values of r_c (Levenspiel, 1999).

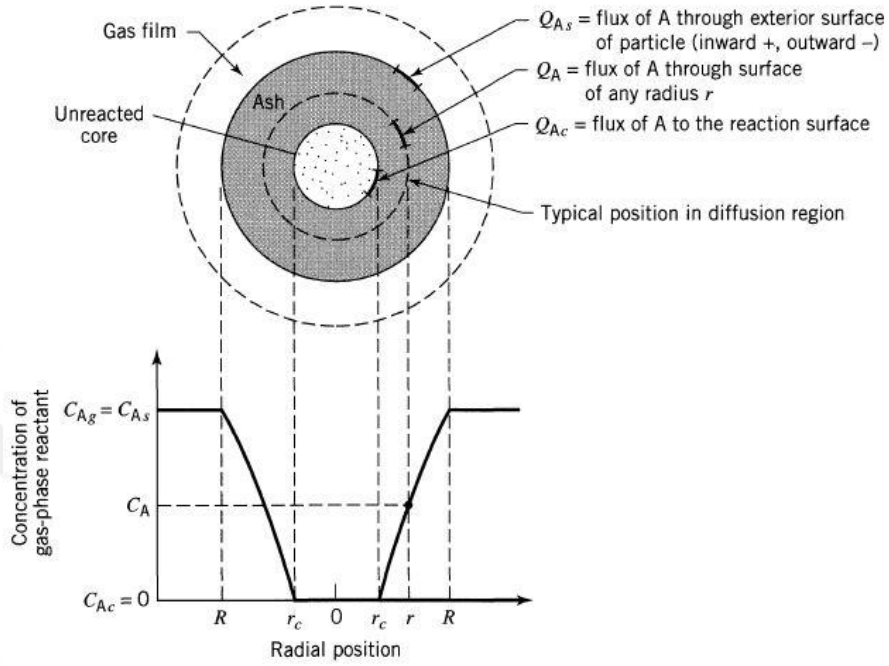

Figure 2.16 Illustration of a reacting particle when diffusion through a product layer is the controlling step (Koech et al., 2014; Levenspiel, 1999)

The reaction rate of Reactant A is calculated by the diffusion rate at the reaction surface at any given time. The calculations is realized by using Equation 2.5 where Q_A is the flux, N_A is the number of moles, and the t represents time, Q_{Ac} is the flux of A to the reaction surface, Q_{Ac} it the flux of A through exterior surface of particle, R is the diameter of particle, r is the radius of particle (Gupta, 2006; Koech et al., 2014; Safari et al., 2009; Sohn et al., 1979).

$$-\frac{dN_A}{dt} = 4\,\pi\,r^2 Q_A = 4\,\pi\,R^2 Q_{As} = 4\,\pi\,r^2 Q_{Ac} = Constant \qquad (2.5)$$

The flux of A within the product layer can be expressed by the Fick's law for equimolar counter diffusion and then Equation 2.6 was achieved (Gupta, 2006; Koech et al., 2014; Safari et al., 2009; Sohn et al., 1979).

$$Q_A = D_e \frac{dC_A}{dr} \tag{2.6}$$

In Equation 2.6, D_e is the effective diffusion coefficient of gaseous reactant in the product layer. With the combining of Equation 2.5 and 2.6, Equation 2.7 is obtained (Koech et al., 2014).

$$-\frac{dN_A}{dt} = 4\,\pi\, r^2 D_e \frac{dC_A}{dr} = Constant \tag{2.7}$$

The integration of Equation 2.7 across the product layer form R to r_c is gives to Equation 2.8 (Koech et al., 2014). The Equation 2.8 represents the conditions of a reacting particle at any time. In this equation, C_{Ag} represents of reactant concentration of particle surface.

$$-\frac{dN_A}{dt}\left(\frac{1}{r_c} - \frac{1}{R}\right) = 4\,\pi D_e C_{Ag} \tag{2.8}$$

The second part includes the size of an unreacted core changed with time. In this part, the size of the unreacted core is constant; however, the product layer becomes thicker. As a result, integration of Equation 2.8 with according to time and other variables should yield the required relationship. But, this new equation contains three variables that must be eliminated or rewritten in terms of the other variables before integration. These three variables are *t*, N_a and r_c. First, N_a can be written in terms of r_c and equation 2.9 can be achieved (Koech et al., 2014).

$$-\rho_B \int_{r_c=R}^{r_c} \left(\frac{1}{r_c} - \frac{1}{R}\right) r_c^2 dr_c = b D_e C_{Ag} \int_0^t dt \tag{2.9}$$

Or

$$t = \frac{\rho_B R^2}{6bD_e C_{Ag}} \left[1 - 3\left(\frac{r_c}{R}\right) + 2\left(\frac{r_c}{R}\right)^3\right] \quad (2.10)$$

The ρ_B represents solid particle molar density. For the complete conversion of a particle, when $r_c = 0$, the duration is found by using Equation 2.11.

$$\tau = \frac{\rho_B R^2}{6bD_e C_{Ag}} \quad (2.11)$$

The progression of reaction in terms of the time required for complete conversion is found by dividing Equation 2.11 and Equation 2.10.

$$\frac{t}{\tau} = 1 - 3(1 - R)^{2/3} + 2(1 - R) \quad (2.12)$$

Equation 2.12 is utilized when the diffusion through a product layer is the controlling mechanism (Gupta, 2006; Koech et al., 2014; Lim et al., 2016; Safari et al., 2009; Sohn et al., 1979).

2.3.5.2 Chemical Reaction is the Controlling Mechanism

Figure 2.17 represents when the chemical reaction is the controlling mechanism. The illustration shows the concentration gradient of the particle. The conversion rate becomes proportional to the surface area of the unreacted nucleus if the reaction is not affected by the diffusion through a product layer. Therefore, the rate of reaction for unit surface of the unreacted core (r_c) is given in Equation 2.13 (Gupta, 2006; Koech et al., 2014; Safari et al., 2009; Sohn et al., 1979).

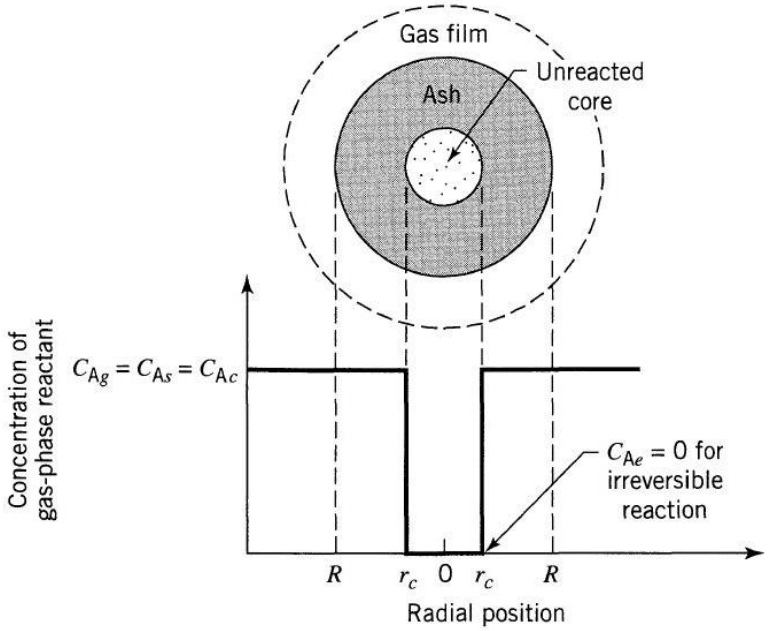

Figure 2.17 Illustration of reaction particle when chemical reaction is the controlling mechanism (Koech et al., 2014)

In the Equation 2.13, k'' is the first-order rate constant for the surface reaction. N_B represents the term of shrinking radius, and N_b can be rewritten as in the Equation 2.14 (Gupta, 2006; Koech et al., 2014; Safari et al., 2009; Sohn et al., 1979).

$$-\frac{1}{4\pi r_c^2}\frac{dN_B}{t} = -\frac{b}{4\pi r_c^2}\frac{dN_B}{dt} = bk''C_{Ag} \tag{2.13}$$

$$-\frac{1}{4\pi r_c^2}\rho_b 4\pi r_c^2 \frac{dr_c}{dt} = -\rho_b \frac{dr_c}{dt} = bk''C_{Ag} \tag{2.14}$$

After integration of Equation 2.14, Equation 2.15 is obtained.

$$-\rho_B \int_R^{r_c} dr_c = bk''C_{Ag} \int_0^t dt \tag{2.15}$$

Or

$$t = \frac{\rho_B R^2}{bk''C_{Ag}}(R - r_c) \tag{2.16}$$

The required duration for the complete conversion (τ) is found when r_c= 0, and Equation 2.17 is obtained:

$$\tau = \frac{\rho_B R}{bk'' C_{Ag}} \tag{2.17}$$

The decreasing in radius or increasing in fraction conversion of the particle, in terms of τ, is found by combining both Equation 2.16 and 2.17. Thus, Equation 2.18 was obtained (Gupta, 2006; Koech et al., 2014; Safari et al., 2009; Sohn et al., 1979).

$$\frac{t}{\tau} = 1 - \frac{r_c}{R} = 1 - (1 - R)^{1/3} \tag{2.18}$$

2.4. Literature Reviews

In recent years, many researchers have studied about leaching kinetics of raw materials containing REEs. These studies have investigated the effects of different types of acid solutions, different ores, REEs containing slags and scraps as a source, REEs concentration, acid concentrations, and leaching duration on the leaching kinetics.

Bian et al. investigated the leaching kinetics of bastnasite concentration. The bastnasite ore contains of 71.4 mass % REOs. In that study, the effects of different leaching temperature, HCl acid concentration, liquid/solid ratio, and particle size were investigated. They used the shrinking core model for the determination of the leaching kinetics. The rate-controlling steps were determined as diffusion through a product layer. The activation energies were calculated 59.39 kJ/mol for REEs, according to the Arrhenius equation (Xue, Yin, Yao, & Wu, 2011).

Feng et al. also investigated leaching kinetics studies of REEs from bastnasite ore. They used bastnasite ore as a raw material. In their study, the effects of stirring rate,

H_2SO_4 acid concentration, leaching temperature, particle size of ores on the leaching kinetic and RE extraction efficiencies were investigated. The optimum conditions for highest RE extraction was found as 0.074-0.100 mm particle size, 1.5 mol/L H_2SO_4 acid concentration, 1/8 solid/liquid ratio and stirring speed of 500 rpm. The shrinking core model was used for the determination of leaching kinetics of REEs. The analysis showed that the diffusion through a product layer was the controlling step. The activation energy of leaching was calculated 9.997 kJ/mol according to the Arrhenius equation (Feng et al., 2013).

Huang et al. investigated the leaching kinetics of REEs and fluoride containing mixed RE concentration. The mixed concentration contains bastnasite and monazite ores. They utilized HCl-$AlCl_3$ solutions for leaching. To determine the leaching kinetics, the effects of HCl acid concentration, leaching temperature, leaching duration, solid/liquid ratio, $AlCl_3$ concentration, and stirring speed were investigated. The optimum conditions were found as 3 mol/L HCl concentration, 0.5 mol/L $AlCl_3$ concentration, 70 ℃ leaching temperature, 10 mL/g liquid/solid ratio, 300 rpm stirring speed and 40 minutes leaching duration, respectively. The shirking core model was applied for the determination of the leaching mechanism. The leaching mechanism was found as mixed controlled (chemical reaction and diffusion through a product/ash layer) for both REEs and fluoride. And, the calculated activation energies were found as 26.95 kJ/mol for REEs and 20.70 kJ/mol for fluoride, respectively (Huang et al., 2017).

The leaching kinetics of Korean monazite ore, which is another critical REEs ores, were investigated by Panda et al. The method of their study was started with dephosphorization by using NaOH (50% w/v) digestion at 170 ℃, and 100 g/L solid/liquid ratio in 4 h. The leaching kinetics of phosphate was found as chemical reaction controlled. Furthermore, 6 N HCl acid concentration at 90 ℃ leaching temperature with 60 g/L solid/liquid ratio for two h leaching duration was used for leaching of rare earth hydroxide. 99.99% of phosphate and 95% of REEs recovered. The leaching kinetics of phosphate was found as chemical reaction controlled and

58.04 kJ/mol of activation energy was calculated according to the Arrhenius equation (Panda et al., 2014).

Kinetic studies were also investigated for leaching of REEs containing slags. Kim et al. investigated the leaching kinetics of lanthanum from magnetite ore containing monazite. The optimum conditions were determined at 1.5 g slag per L of 0.3 M H_2SO_4 acid solutions at 80 ℃ leaching temperature with 750 rpm stirring speed. The shrinking core model for a spherical particle of unchanging size was applied on the slags for the determination of leaching kinetics. The analysis results showed that there were two stages in leaching parts, the first step was controlled by the chemical reaction and the second step was controlled by the diffusion through a product layer. The Arrhenius equation were used to calculate the activation energies. The calculated activation energy for reaction controlled was 10.0 kJ/mol and the activation energy for diffusion through a product layer was 24.8 kJ/mol (Yoon et al., 2015).

Jun et al. investigated the leaching kinetics of weathered crust elution-deposited rare earth ores with ammonium sulfate solution. The study showed that when the leaching temperature rose or the particle size decreased, it affected the leaching process in a right way. The shrinking-core model was used for the description of leaching kinetic mechanism. The results showed that the leaching mechanism was controlled by diffusion through a product layer and the calculated activation energy was 9.24 kJ/mol (Jun et al., 2010).

In this study, leaching kinetics of Ce, La, Nd, and Pr were investigated. The method was developed by using the data and models in the literature.

CHAPTER THREE

EXPERIMENTAL STUDIES

3.1 Materials

In the experimental studies, the certified reference material (CRM), Wigu carbonatite complex ores deposited in Wigu Hill, Tanzania, were used as the raw material in leaching experiments. The CRM has a code as AMIS0185 named by Montero Resources limited company. The CRM was prepared by using the carbonatite ores in the region at the Wigu-Hill complex located 200 km southwest of Dar es Salaam city of Tanzania. Wigu-Hill consists of altered sediment rocks containing high-grade leaf granite and amphibolite dating from the Paleoproterozoic period. The CRM has a dolomitic character with a significant amount of rare earth oxide minerals and also contains quartz, barite, strontianite, iron oxide, and minerals containing a small amount of manganese. When looking at minerals containing rare earth elements, the CRM is rich in bastnasite and consists small amount of synchysite, parasite, monazite, and a trace amount of apatite. The REEs in these minerals are heavily light rare earth elements, including cerium (Ce), lanthanum (La), neodymium (Nd), praseodymium (Pr), and samarium (Sm). A small amount of Europium (Eu) and gadolinium (Gd) are also included in the content, but other rare earth elements were found in trace amounts. The CRM has a specific weight of 3.28 g/cm^3 with under 54 μm particle size. According to the results of wet sieve analysis, 98.5% of the CRM are under 54 μm particle size.

Analytical grade acid solutions (70% v/v HNO_3 and 37% v/v HCl) by Merck and distilled water were used for preparing of leaching solutions. A thermocouple was used to measure leaching temperature and a hot plate with magnetic stirrer (Heidolph) was used to keep the stirring speed of the acid solution constant.

3.2 Method

The acid solution was prepared for the leaching process and then the CRM were charged into the prepared solutions and the leaching mechanism was determined by examining the amounts of the REEs dissolved at varying leaching temperature and duration. The leaching experiments were started with the mixing of the CRM with the acid solution that heated up to selected temperature in a beaker on a magnetic stirrer. During the experiment, the temperature of the solution was measured and fixed with a thermocouples connected to the magnetic stirrer. After leaching, the solid-liquid separation was carried out using a filter paper (Sartorius, Grade 391) with using a vacuum pump and a glass flask (1000 mL). After solid-liquid separation, the filter cake was washed with distilled water to remove the acid residue. The loaded acid solution was stored in a 250 mL glass flask. The leaching mechanisms were determined by examining the effects of leaching temperatures (25 – 40 – 60 °C) and leaching duration (10 – 15 – 30 – 45 – 60 min) on the leaching efficiencies. In the leaching experiments, 3 M of acid solutions (HCl and HNO_3) with 100 ml volume, 5 g of CRM, and 400 rpm stirring rate were kept constant. The schematic drawing of the leaching experiments was given in Figure 3.1.

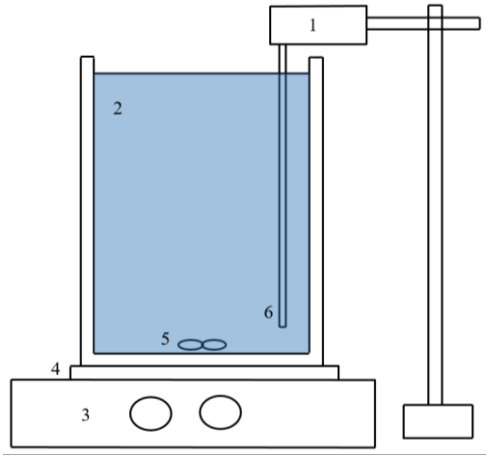

Figure 3.1 The schematic drawing of the leaching experiments (1. Temperature display, 2. Acid solution, 3. Magnetic stirrer, 4. Hot plate, 5. Magnet, 6. Thermocouple).

The loaded solutions obtained after solid-liquid separation were analyzed by La, Ce, Nd, and Pr analysis by Agilent 720 series Radial ICP-OES to determine the chemical compositions.

The shrinking core model was used to determine the leaching kinetics of Ce, La, Nd, and Pr because of the non-porous particle structure of the CRM.

The results of the chemical analysis obtained by leaching at different temperature and durations were used to plot the graphs for kinetic calculations. The linear regression model was used to calculate the rate constants of diffusion and chemical reaction controlled systems (k_d and k_r), the correlation coefficients (R^2) and the activation energies of system.

CHAPTER FOUR

RESULTS AND DISCUSSION

4.1 Raw material analysis results

The compositions of certified reference materials (CRM) were analyzed by 18 independent organizations, and the mean values of the elements and compounds in the CRM are given in Table 4.1. The X-ray diffraction analysis result of the CRM is given in Figure 4.1. The CRM contains 8.38 mass% REEs (or 10.05 mass% RE-oxides). The CRM contains mainly dolomite, quartz, and RE-oxide minerals (Bastnasite, parasite, monazite) with a few amount of barite and iron oxide minerals.

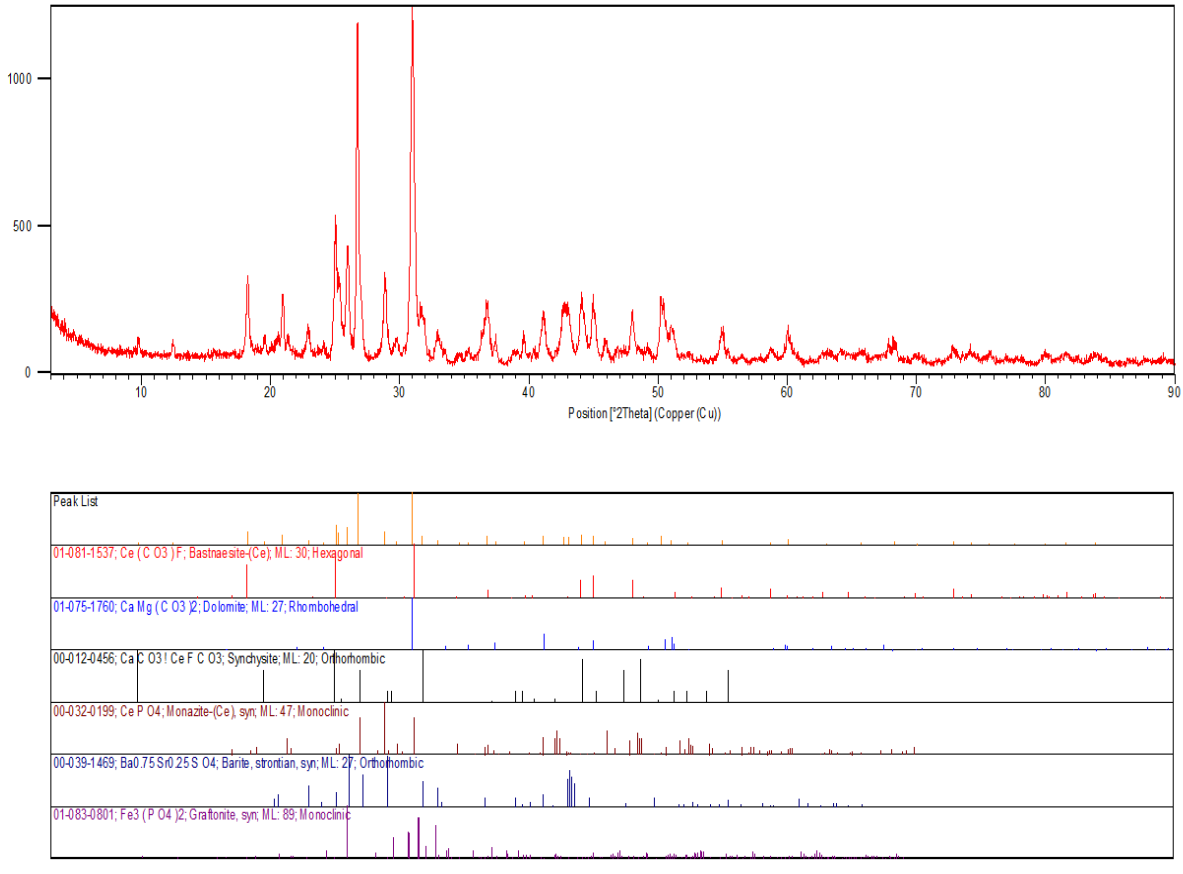

Figure 4.1 XRF analysis of the standard reference materials used as raw material

Table 4.1 Chemical composition of the standard reference materials used as raw material

Element	**Ce (ICP)**	**Ce (XRF)**	**La (ICP)**	**La (XRF)**	**Nd (ICP)**	**Pr (ICP)**	**Sm (ICP)**	**Other REEs (ICP)**
Amount	%4.07 ± 0.461	% 4.15 ± 0.61	% 2.97 ± 0.27	% 3.00 ± 0.17	9238 ppm ± 103	3471 ppm ± 343	556 ppm ± 48	469 ppm ± 25,5
Compound	**Al_2O_3 (XRF)**	**CaO (XRF)**	**Fe_2O_3 (XRF)**	**MgO (XRF)**	**P_2O_5 (XRF)**	**SiO_2 (XRF)**	**MnO (XRF)**	**Loss of ignitions**
Amount	% 2.22 ± 0.12	% 11.48 ± 0.36	% 5.29 ± 0.28	% 4.65 ± 0.20	% 1.74 ± 0.10	% 21.53 ± 0.82	% 1.09 ± 0.16	% 20.69 ± 0.64

4.2 Leaching Results

In the first leaching experiment, different acid concentrations were determined to obtain optimum conditions.

The chemical compositions of the loaded solutions obtained with different acid concentrations at room temperature is given in Table 4.2. The dissolved amount of Ce, La, Nd, and Pr were increased with increasing in acid concentrations. The higher amounts of dissolved Ce, La, Nd and Pr were obtained by using HNO_3 acid solutions. With the increasing in acid concentrations, the dissolved amounts of elements other than REEs were increased rapidly than REEs. Due to the ratio of dissolved amount of REEs to non-REEs, the optimum acid concentration was decided as 3 M. It was also selected due to consideration of the environmental factors and costs.

Equation 4.1 was used for calculation of conversion rate in metallurgical process kinetic. The leaching duration and calculated recovery values given in Table 4.3. By using chemical analysis results and Equation 4.1, the leaching behavior of Ce, La, Nd, and Pr in CRM were calculated and results given in Figure 4.3 for HNO_3 acid solution, and Figure 4.3 for HCl acid solution.

Table 4.2 Amounts of dissolved REEs in the loaded solutions obtained by different acid concentration at room temperature.

Acid Type	**Concentration (M)**	**Amount of dissolved metal in solutions (ppm)** Ce	La	Nd	Pr
HCl	**1**	21.63	9.78	4.96	1.53
	2	28.33	15.17	7.08	2.19
	3	32.59	18.61	8.21	2.65
	4	29.21	16.70	7.45	2.41
	5	35.06	21.58	9.34	3.11
	6	34.76	21.23	9.38	3.07
	7	36.92	22.30	10.08	3.29
	8	36.00	22.13	9.84	3.25
HNO_3	**1**	23.97	11.25	5.52	1.72
	2	32.28	17.94	8.13	2.60
	3	31.18	18.40	8.02	2.62
	4	34.26	20.62	8.99	2.95
	5	34.01	21.10	9.21	3.03
	6	37.57	23.37	10.16	3.35
	7	37.34	23.24	10.33	3.41
	8	35.28	21.84	9.66	3.19

Table 4.3 Calculated Recovery Values

Acid Type	Leaching Duration (min.)	Recovery Value Ce	La	Nd	Pr
HCl	10	21.1	18.7	28.4	21.7
	15	20.5	18.3	27.8	21.1
	30	24.3	22.0	33.6	25.9
	45	24.3	22.1	33.5	25.8
	60	26.2	24.0	36.1	28.1
HNO_3	10	15.9	14.3	22.5	17.1
	15	16.9	15.1	23.7	18.3
	30	18.0	16.4	25.3	19.4
	45	20.8	19.0	29.0	22.3
	60	21.2	19.4	29.7	22.8

$$\boldsymbol{Reaction\ rate} = \frac{\boldsymbol{Amount\ of\ conversion\ material}}{\boldsymbol{Observation\ Time}} \quad (4.1)$$

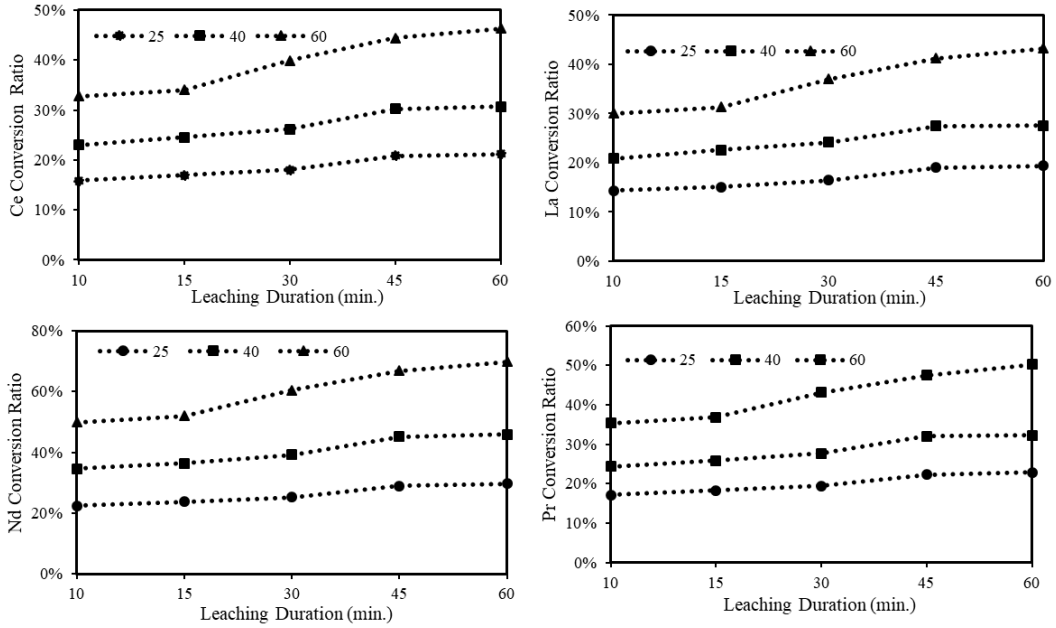

Figure 4.3 Conversion ratio of Ce, La, Nd and Pr at different leaching durations and temperatures using 3M HNO_3 acid solutions (●, ■, and ▲ represent leaching temperature at 25, 40 and 60 °C, respectively)

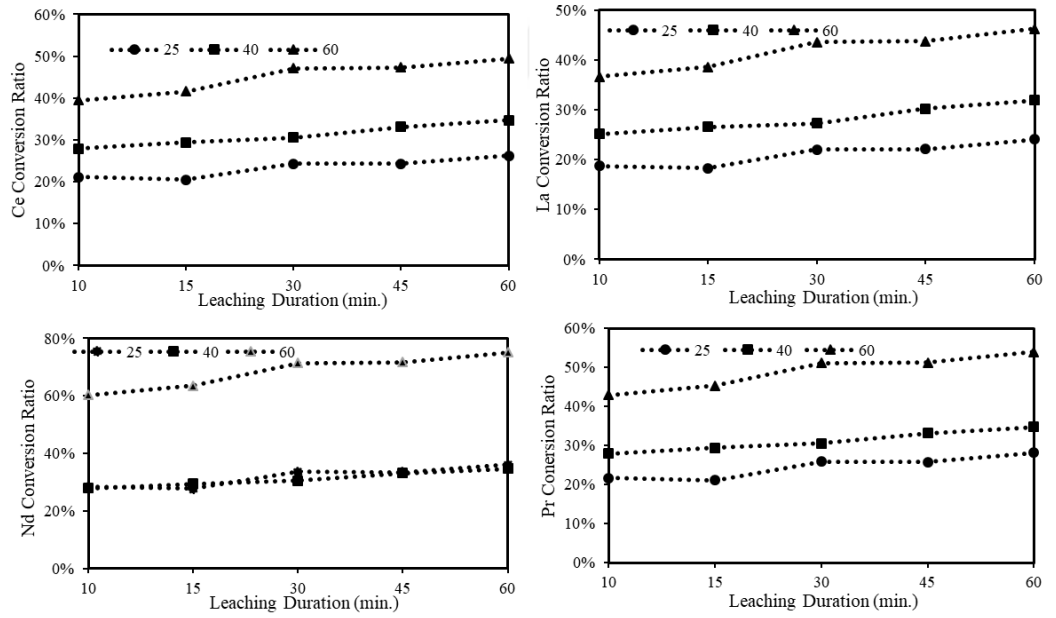

Figure 4.3 Conversion ratio of Ce, La, Nd and Pr at different leaching durations and temperatures using 3M HCl acid solutions (●, ■, and ▲ represent leaching temperature at 25, 40 and 60 °C, respectively)

According to the calculation, increases in the leaching duration and leaching temperature had a positive effect on the conversion rate of REEs. The highest

conversion rates for Ce, La, Nd, and Pr were observed during 60 min leaching at 60 ℃ with using 3M HCl acid solutions. The conversion rates were obtained 46% for Ce, 43% for La, 70% for Nd, and 50% for Pr, respectively.

Both HCl acid solution and HNO_3 acid solution behaviors were similar. In other words, as the leaching temperature and leaching duration increased, the conversion rates were also increased for both acid solutions. The highest conversion rates for Ce, La, Nd, and Pr were observed during 60 min leaching at 60 ℃ with using 3M HNO_3 acid solutions. The conversion rates were obtained 49% for Ce, 46% for La, 75% for Nd, and 54% for Pr, respectively. When the conversion rates of Ce, La, Nd, and Pr in both acids were compared, HNO_3 acid solutions were better than HCl acid solution at all leaching temperatures and durations.

In the shrinking core model, if the process rate is controlled by the chemical reactions Equation 4.2 is used for calculating the process rate and the completion duration. The values obtained from conversion ratios were used in the Equation 4.2 indicated as *R*. The linear regression analysis of leaching durations vs $1–(1–R)^{1/3}$ values gives us the process rate. By drawing of $1–(1–R)^{1/3} – t$ diagram, the rate constant of chemical reaction controlled process (k_r) can be calculated from the slope of the diagram. The conversion values of REEs obtained by the leaching of different temperature and durations were used to plot the diagrams. The process rates controlled by the chemical reaction were given in Figure 4.5 for HNO_3 and Figure 4.6 for HCl acid solutions.

$$k_r \times t = 1 - (1 - R)^{1/3} \tag{4.2}$$

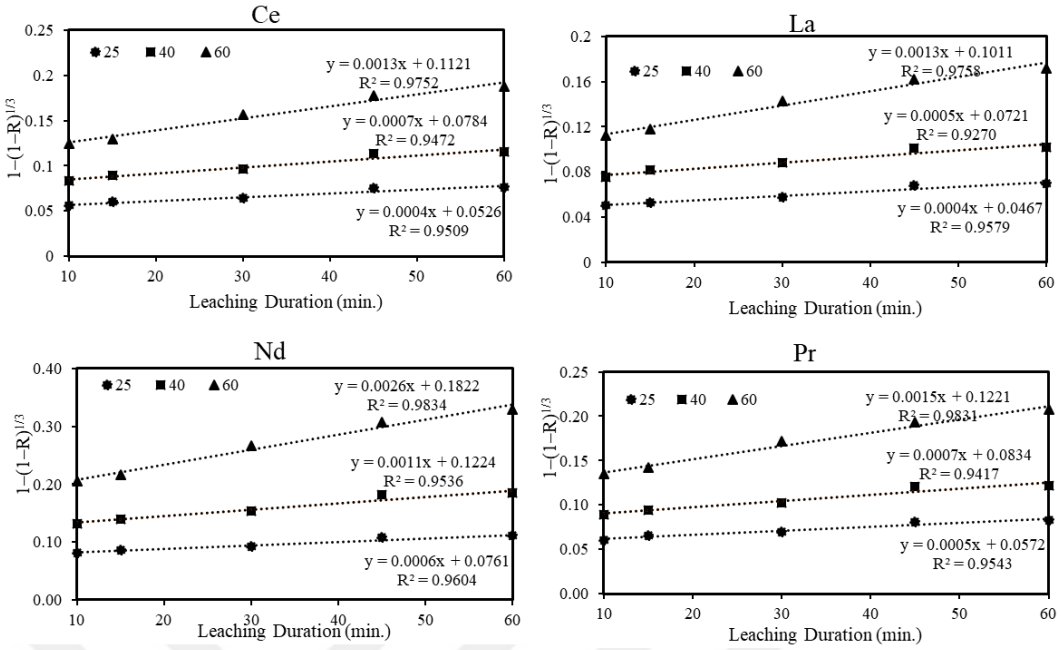

Figure 4.5 The relationship between $1–(1–R)^{1/3}$ and leaching duration at different temperatures calculated by the conversion of Ce, La, Nd, and Pr in 3M HNO_3 acid solutions (●, ■, and ▲ represent leaching temperature at 25, 40 and 60 °C, respectively)

The comparison of Figure 4.4 and 4.5 showed that, the determination coefficients (R^2) of the linear regression measured for leaching with HNO_3 acid solution were more close to the unity than HCl acid solutions. For statistically, the linearity was increased by increasing in leaching temperatures. The highest determination coefficients were calculated by dissolution of Nd by both of the acid solutions.

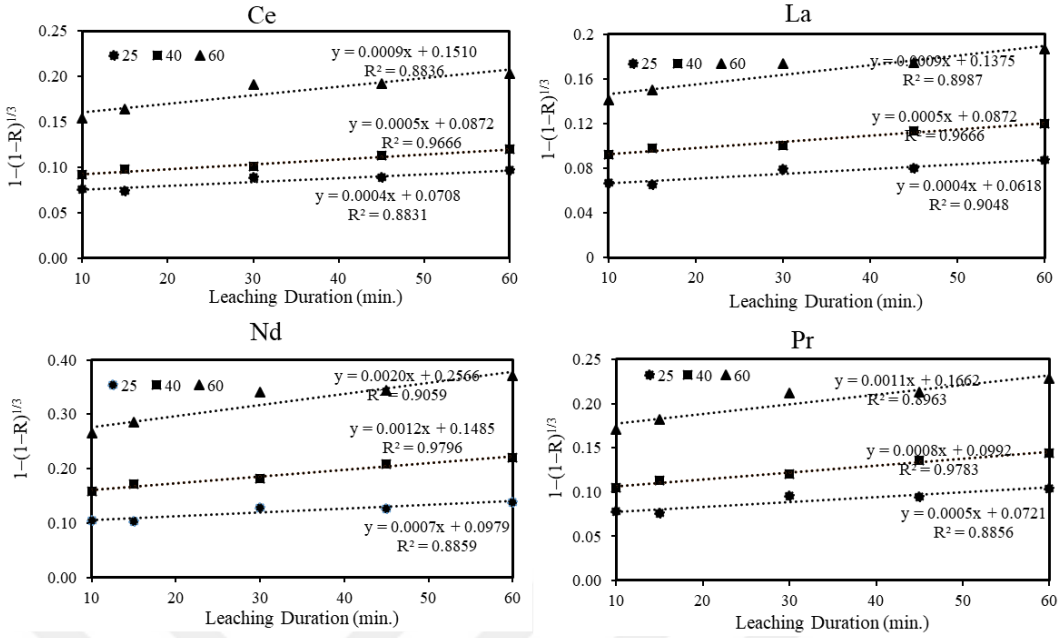

Figure 4.6 The relationship between $1–(1–R)^{1/3}$ and leaching duration at different temperatures calculated by the conversion of Ce, La, Nd, and Pr in 3M HCl acid solutions (●, ■, and ▲ represent leaching temperature at 25, 40 and 60 °C, respectively)

In the shrinking core model, if the process rate is controlled by the diffusion through a product layer Equation 4.3 is used for calculating the process rate and the completion duration. The values obtained from conversion ratios were used in the Equation 4.3 indicated as *R*. The linear regression analysis of leaching durations vs $1–3(1–R)^{2/3}+2(1–R)$ values gives us the process rate. By drawing of $[1–3(1–R)^{2/3}+2(1–R)] – t$ diagram, the rate constant of the diffusion through a product layer controlled process (k_d) can be calculated from the slope of the diagram. The conversion values of REEs obtained by the leaching of different temperature and durations were used to plot the diagrams. The process rates controlled by the chemical reaction were given in Figure 4.7 for HNO_3 and Figure 4.8 for HCl acid solutions.

$$k_d \times t = 1 - 3(1 - R)^{2/3} + 2(1 - R) \quad (4.3)$$

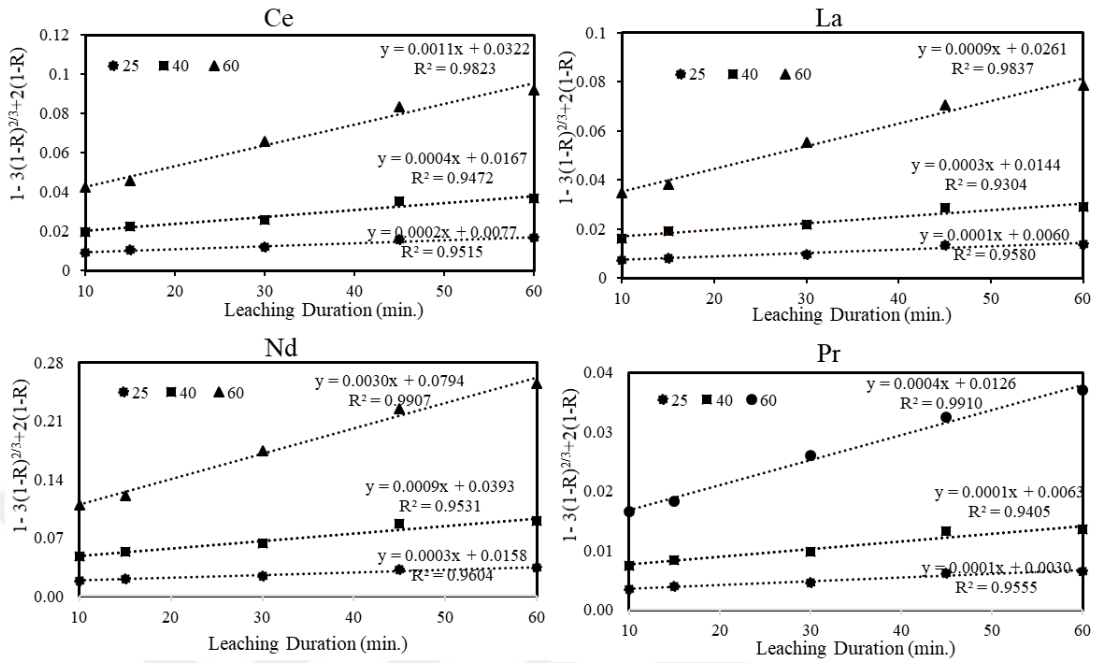

Figure 4.7 The relationship between 1- $3(1-R)^{2/3}+2(1-R)$ and leaching duration at different temperatures calculated by the conversion of Ce, La, Nd, and Pr in 3M HNO_3 acid solutions (●, ■, and ▲ represent leaching temperature at 25, 40 and 60 °C, respectively)

The comparison of the determination coefficient calculated due to the shrinking core model respecting to be controlled by both chemical reaction and diffusion through a product layer was given in Table 4.4, obtained by the leaching of REEs with the solutions containing 3 M acid concentration.

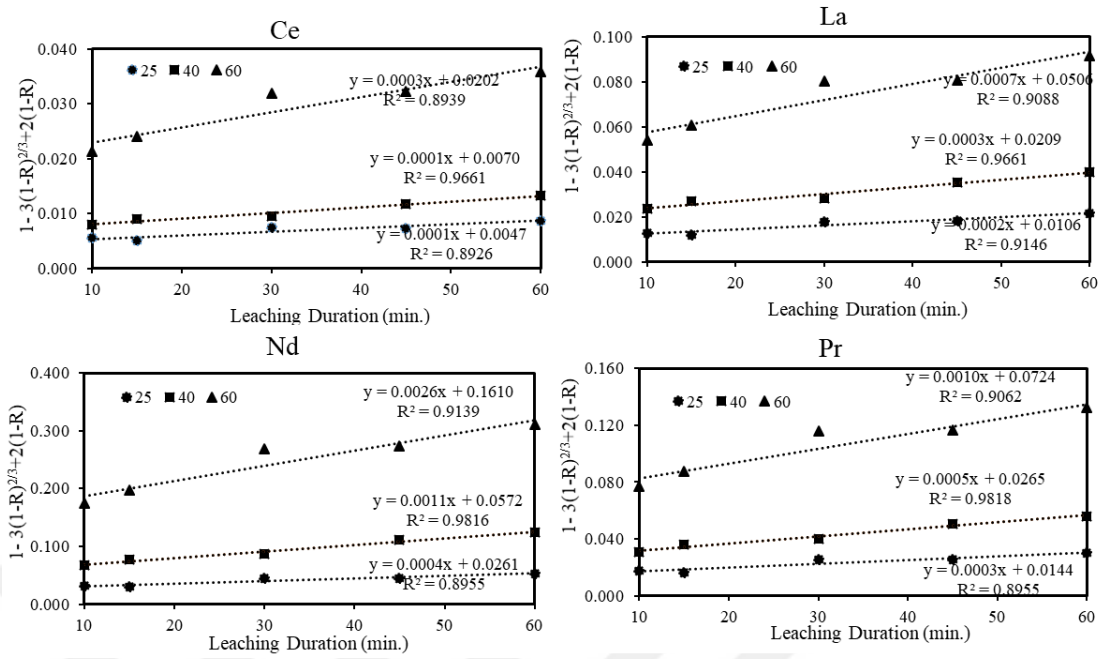

Figure 4.8 The relationship between 1- $3(1-R)^{2/3}$+2(1-R) and leaching duration at different temperatures calculated by the conversion of Ce, La, Nd, and Pr in 3M HCl acid solutions (●, ■, and ▲ represent leaching temperature at 25, 40 and 60 °C, respectively)

Table 4.4 The comparison of the determination coefficients of the controlling mechanisms of REEs leaching by using different acid solutions at different temperatures.

Acid Type	HNO_3						HCl					
Mechanism	Reaction			Diffusion			Reaction			Diffusion		
Temp. °C	25	40	60	25	40	60	25	40	60	25	40	60
Ce	0.95	0.95	0.98	0.94	0.99	0.98	0.88	0.97	0.88	0.89	0.97	0.89
La	0.96	0.92	0.98	0.96	0.93	0.98	0.90	0.97	0.90	0.91	0.97	0.91
Nd	0.96	0.95	0.98	0.96	0.95	0.99	0.88	0.98	0.91	0.90	0.98	0.91
Pr	0.95	0.94	0.98	0.96	0.94	0.99	0.89	0.98	0.90	0.90	0.98	0.91

It was seen from Figure 4.4 to Figure 4.7, the similar conversion rates were obtained from the plots. To find the slope of the data, linear regression analysis, one of the least-squares regression techniques, was applied. The coefficients of determination (R^2) calculated as a result of linear regression error approximate zero as the coefficient of

determination approach 1, thus the obtained line explains 100% of the variability of the data (Chapra, S., & Canale, 2011).

When the determination coefficient values were examined, it was observed that both mechanisms (chemical reaction and diffusion) showed a dynamic character to the reaction rate. This kind of process was referred as mixed controlled. The controlling mechanisms of the process rates can be also determined by the activation energies of the processes. The comparison of the controlling mechanisms and their activation energy values was given in Table 4.5 (Sohn et al., 1979).

Table 4.5 Control mechanisms, slowest step, and their activation energies (Sohn et al., 1979)

Control mechanism	Slowest step	Activation energy
Reaction Controlled	Chemical reaction	$> 40\ kJ$/mol
Diffusion Controlled	Diffusion	$E < 20\ kJ/mol$
Mixed controlled	Indistinguishable	$20 < E < 40\ kJ/mol$

The activation energies of the processes were calculated due to the Arrhenius equation given in Equation 4.4 (and Equation 4.5), where both k_d and k_r values obtained from the slopes of the graphs given in Figure 4.4 to Figure 4.7 were used.

$$\boldsymbol{k = A \exp[-E_A\ /(RT)]} \tag{4.4}$$

$$\boldsymbol{ln\ k = ln\ A - \frac{E_A}{R} \cdot \frac{1}{T}} \tag{4.5}$$

Due to the Arrhenius equation, for the calculation of activation energy, a linear regression must be realized between ln *k to* 1/*T*. The slope of the linear function gives– E_A/R values. Firstly, k_d values obtained from the leaching process were used for the activation energy calculations. The graphs plotted in order to the Arrhenius equation were given in Figure 4.9 for HNO_3 and in Figure 4.10 for HCl acid leaching.

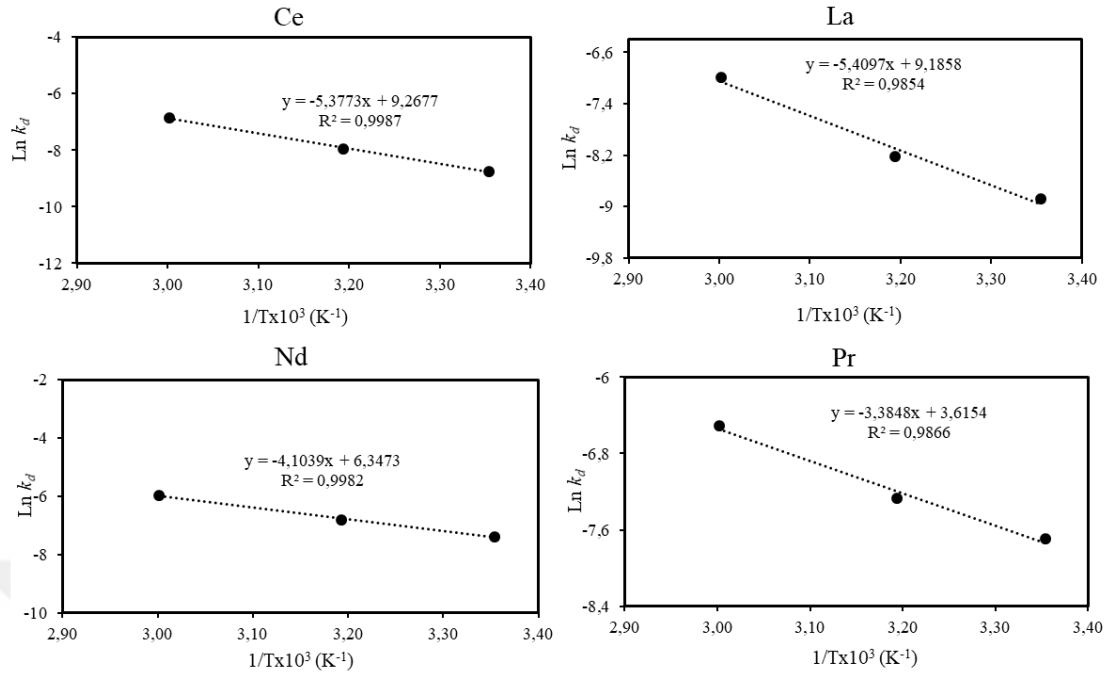

Figure 4.9 The linear regression results of ln k_d vs 1/T for REEs dissolution in 3 M HNO_3 acid solutions

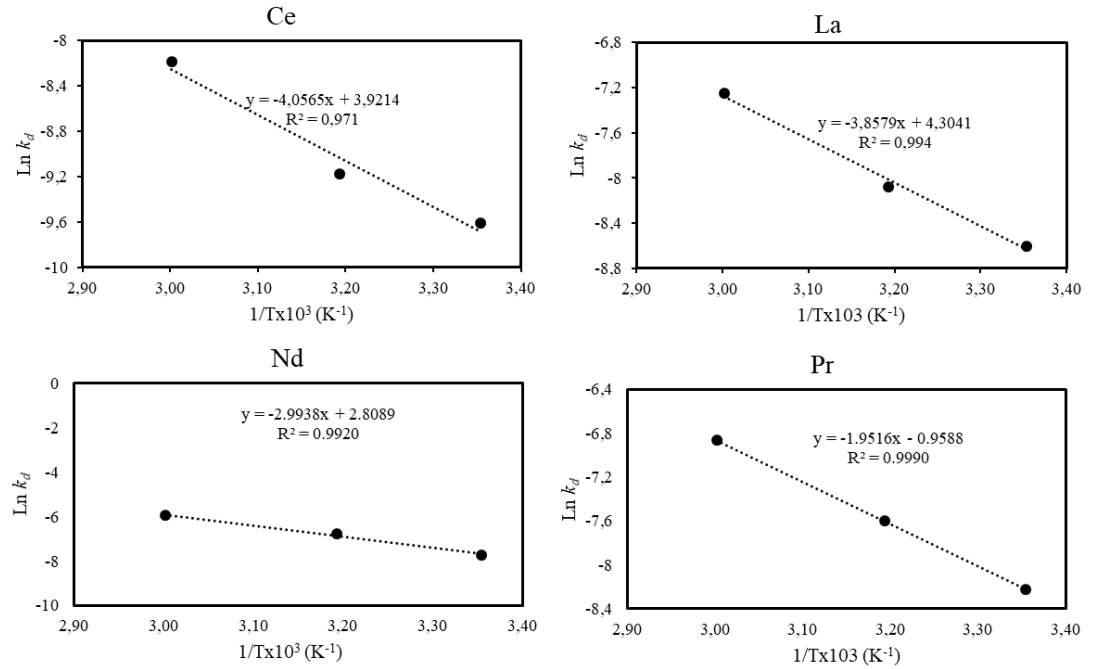

Figure 4.10 The linear regression results of ln k_d vs 1/T for REEs dissolution in 3 M HCl acid solutions

The activation energy values of the leaching process of the Ce, La, Nd, and Pr elements in the 3M acid solutions were calculated by using the Arrhenius equation and the slope of the linear regressions were given in Table 4.6.

Table 4.6 Calculated activation energies of REEs leaching with different acid solutions where the process was controlled by diffusion through a product layer

Elements	Activation Energies (kJ/mol)	
	HCl acid solution	HNO_3 acid solution
Ce	33.72	44.70
La	32.07	44.97
Nd	41.72	53.03
Pr	32.06	45.73

Comparing of the calculated activation energies given in Table 4.6 and Table 4.5, it was found that, the leaching of REEs in HNO_3 acid solutions should be controlled by chemical reaction. Also, the leaching of Nd in HCl acid solution should be also controlled by chemical reaction, while the leaching of Ce, La and Pr should be mixed controlled (both chemical reaction and diffusion through a product layer).

On the other hand, k_r values obtained from the leaching process were also used for the activation energy calculations. The graphs of the linear regressions of ln k_r vs $1/T$ were given in Figure 4.11 for HNO_3 and Figure 4.12 for HCl acid solutions.

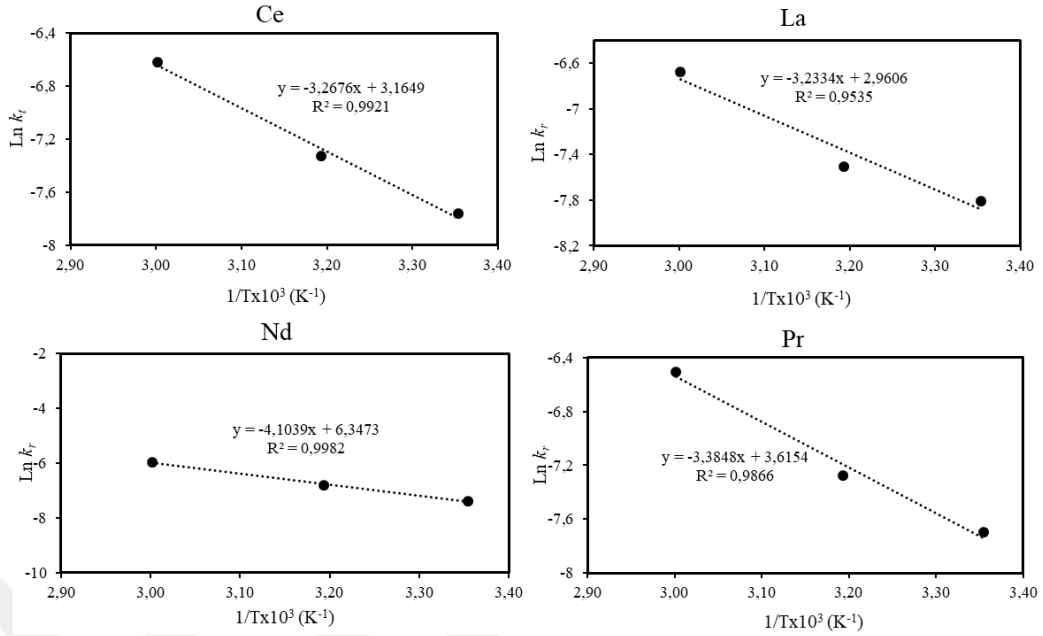

Figure 4.11 The linear regression results of ln k_r vs 1/*T* for REEs dissolution in 3 M HNO_3 acid solutions

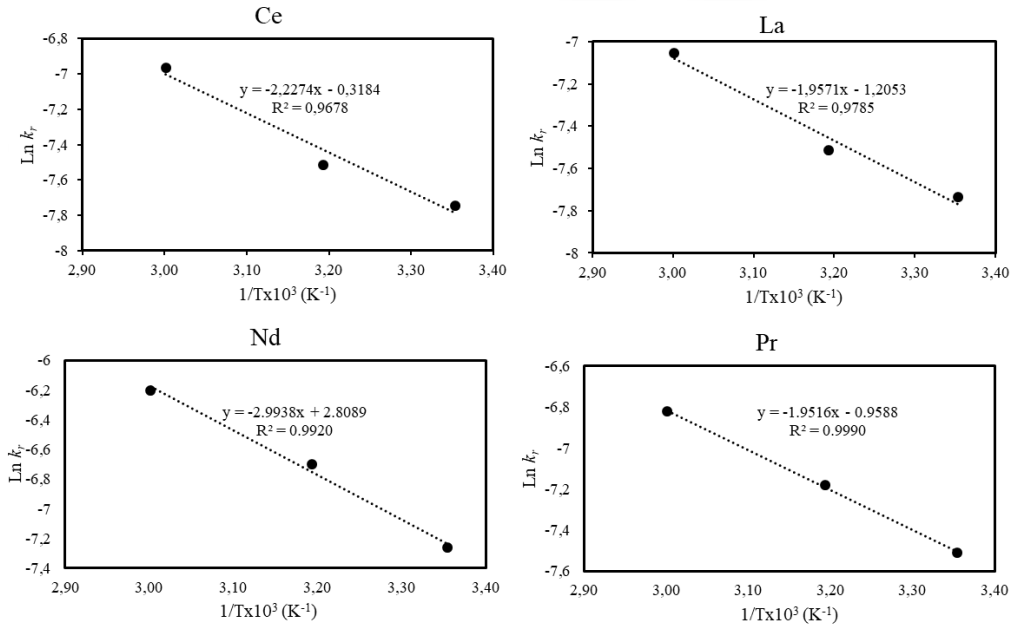

Figure 4.12 The linear regression results of ln k_r vs 1/*T* for REEs dissolution in 3 M HCl acid solutions

The activation energy values of the leaching process of the Ce, La, Nd, and Pr elements in the 3M acid solutions were calculated by using the Arrhenius equation and the slope of the linear regressions were given in Table 4.7.

Table 4.7 Calculated activation energies of REEs leaching with different acid solutions where the process was controlled by chemical reaction

Elements	Activation Energies (kJ/mol)	
	HCl acid solution	HNO_3 acid solution
Ce	18.52	27.16
La	16.27	26.88
Nd	24.90	34.12
Pr	16.22	28.14

Comparing of the calculated activation energies given in Table 4.7 and Table 4.5, it was found that, the leaching of REEs in HNO_3 acid solutions were mixed controlled (both chemical reaction and diffusion through a product layer). Also, the leaching of Nd in HCl acid solution was mixed controlled, while the leaching of Ce, La and Pr were controlled by diffusion through a product layer.

Due to the assumptions of controlling mechanisms, it can be said that, the leaching process of REEs in CRM was mixed controlled. Thus, increasing of leaching temperature and stirring speed will increase the leaching efficiencies.

CHAPTER FIVE

CONCLUSIONS

In this study, kinetic calculations were investigated to determine the mechanism of leaching process of a certified reference material containing rare-earth elements, Wigu carbonatite complex ores deposited in Wigu Hill, Tanzania. In the leaching experiments, the CRM were dissolved in both HCl and HNO_3 acid solutions. The effects of different leaching durations and leaching temperatures on the leaching behaviors were investigated.

The conversion rates of REEs leached in HCl and HNO_3 acid solutions were calculated by using the plots obtained from the chemical analysis results. The highest conversion rates for Ce, La, Nd, and Pr were observed during 60 min leaching at 60 ℃ with using 3M HCl acid solutions. The conversion rates were measured as 46% for Ce, 43% for La, 70% for Nd, and 50% for Pr, respectively. The highest conversion rates for Ce, La, Nd, and Pr were observed in during 60 min leaching at 60 ℃ with using 3M HNO_3 acid solutions. These conversion rates were measured as 49% for Ce, 46% for La, 75% for Nd, and 54% for Pr, respectively. According to the calculations, increases in the leaching duration and leaching temperature had a positive effect on the conversion rate of REEs. When the conversion rates of Ce, La, Nd, and Pr in both acids were compared, HNO_3 acid solutions were better than HCl acid solution at all leaching temperatures and durations.

The shirking core model approach used for the determination of leaching mechanism. The values obtained from conversion ratios were used for the calculation of $1–(1–R)^{1/3}$ and $1–3(1–R)^{2/3}+2(1–R)$ values. The linear regression analysis of leaching durations vs $1–(1–R)^{1/3}$ and leaching durations vs $1–3(1–R)^{2/3}+2(1–R)$ values give us the process rate. All the graphs have similar behaviors for Ce, La, Nd, and Pr at the determination part of leaching kinetic mechanisms. Due to the similarities in the graphs and R^2 values, there wasn't any significant conclusion made to determine the leaching mechanism. Therefore, the activation energies were calculated to determine

the kinetic mechanism. The Arrhenius equation has been used for dissolution of REEs in both HNO_3 and HCl acid solutions.

The activation energy values of the leaching process of La, Ce, Nd, and Pr were calculated on the slopes of the linear regressions drawn both for k_r and k_d values. The activation energies calculated respected to the both diffusion through a product layer and chemical reaction were given in Table 5.1.

Table 5.1 Calculated activation energies by using both assumptions

Elements	Diffusion Through a Product Layer		Chemical Reaction	
	Activation Energies (kJ/mol)		Activation Energies (kJ/mol)	
	HCl acid solution	HNO_3 acid solution	HCl acid solution	HNO_3 acid solution
Ce	33.72	44.70	18.52	27.16
La	32.07	44.97	16.27	26.88
Nd	41.72	53.03	24.90	34.12
Pr	32.06	45.73	16.22	28.14

Due to the assumptions of controlling mechanisms, the leaching process of REEs in CRM was mixed controlled.

REFERENCES

Anwander, R. (1997). Episodes from the history of the rare earth elements. Herausgegeben von C. H. Evans. Kluwer Academic Publishers, Dordrecht, 1996. 240 S., geb. 89.00 £.—ISBN 0–7923–4101–5. *Angewandte Chemie*, *109*(12), 1414–1415.

Atwood, D. A. (2013). *The rare earth elements : fundamentals and applications.* Chichester : John Wiley & Sons Ltd.

Bokstein, B. S., Mendelv, M. I., & Srolovtz, D. J. (2005). *Science, thermodynamics & kinetics in materials*. New York : Oxford University Press.

Chapra, S., & Canale, R. (2011). *Numerical methods for engineers*. New York : McGraw- Hill.

European Comission. (2017). *Study on the review of the list of critical raw materials*. Retrieved September 23, 2020 from https://ec.europa.eu/growth/sectors/raw-materials/specific-interest/critical_en

Feng, X., Long, Z., Cui, D., Wang, L., Huang, X., & Zhang, G. (2013). Kinetics of rare earth leaching from roasted ore of bastnaesite with sulfuric acid. *Transactions of Nonferrous Metals Society of China*, *23*(3), 849–854.

Gamboghi, J. (2019). *Rare-earth statistic and information,* United States Geological Survey. Retrieved September 23, 2020 from https://www.usgs.gov/centers/nmic/rare-earths-statistics-and-information.

Gbor, P. K., & Jia, C. Q. (2004). Critical evaluation of coupling particle size distribution with the shrinking core model. *Chemical Engineering Science*, *59*(10), 1979–1987.

Girgin, İ., Obut, A., & Üçyildiz, A. (2011). Dissolution behaviour of a Turkish lateritic nickel ore. *Minerals Engineering*, *24*(7), 603–609.

Goodenough, K. M., Wall, F., & Merriman, D. (2018). The rare earth elements: demand, global resources, and challenges for resourcing future generations. *Natural Resources Research*, *27*(2), 201–216.

Gupta, C. K. (2006). *Chemical metallurgy: principles and practice*. Mumbai : John

Wiley & Sons.

Havlik, T., (1999). *Hydrometallurgy principles and applications.* New York : CRC Press.

Huang, Y., Dou, Z., Zhang, T. an, & Liu, J. (2017). Leaching kinetics of rare earth elements and fluoride from mixed rare earth concentrate after roasting with calcium hydroxide and sodium hydroxide. *Hydrometallurgy*, *173*, 15–21.

Humphries, M. (2010). *Rare earth elements: the global supply chain.* Washington, U.S.A: Diane Publishing..

Jha, A. (2014). *Rare earth materials: properties and applications*. New York : Taylor and Francis Group

Jun, T., Jingqun, Y., Ruan, C., Guohua, R., Mintao, J., & Kexian, O. (2010). Kinetics on leaching rare earth from the weathered crust elution-deposited rare earth ores with ammonium sulfate solution. *Hydrometallurgy*, *101*(3–4), 166–170.

Kim, C.-J., Yoon, H.-S., Chung, K. W., Lee, J.-Y., Kim, S.-D., Shin, S. M., … Yoo, S.-J. (2014). Leaching kinetics of lanthanum in sulfuric acid from rare earth element (REE) slag. *Hydrometallurgy*, *146*, 133–137.

Koech, L., Everson, R., Neomagus, H., & Rutto, H. (2014). Dissolution kinetics of sorbents and effect of additives in wet flue gas desulfurization. *Reviews in Chemical Engineering*, *30*(6), 553–565.

Krishnamurthy, N., & Gupta, C. K. (2015). *Extractive metallurgy of rare earths*. New York : CRC press.

Levenspiel, O. (1999). *Chemical reaction engineering*. New York : John Wiley & Sons.

Lim, H., Ibana, D., & Eksteen, J. (2016). Leaching of rare earths from fine-grained zirconosilicate ore. *Journal of Rare Earths*, *34*(9), 908–916.

Panda, R., Kumari, A., Jha, M. K., Hait, J., Kumar, V., Rajesh Kumar, J., & Lee, J. Y. (2014). Leaching of rare earth metals (REMs) from Korean monazite concentrate. *Journal of Industrial and Engineering Chemistry*, *20*(4), 2035–2042.

Qi, D. (2018). *Hydrometallurgy of rare earths: Extraction and separation*. Amsterdam : Elsevier

Ray, H. S., & Ray, S. (2018). *Kinetics of metallurgical processes*. Singapore: Springer Singapore.

Richardson, J. F., Harker, J. H., & Backhurst, J. R. (2002). Leaching. C*hemical Engineering*, 502–540.

Rollat, A., Guyonnet, D., Planchon, M., & Tuduri, J. (2016). Prospective analysis of the flows of certain rare earths in Europe at the 2020 horizon. *Waste Management*, *49*, 427–436.

Safari, V., Arzpeyma, G., Rashchi, F., & Mostoufi, N. (2009). A shrinking particle-shrinking core model for leaching of a zinc ore containing silica. *International Journal of Mineral Processing*, *93*(1), 79–83.

Sohn, H. Y., Hong Y., & Wadsworth, M. E. (1979). *Rate processes of extractive metallurgy*. New York : Springer.

Şeşen, M. K. (1998). Metalurjik süreçlerin kinetiği. İstanbul: ITU Kimya-Metalurji Fakültesi, Ofset Atölyesi.

Vignes, A. (2013). *Extractive metallurgy 1: basic thermodynamics and kinetics*. Hoboken : John Wiley & Sons .

Voncken, J. H. L. (2016). The rare earth elements: An introduction. Cham: Springer.

William D Callister Jr. (2013). *Fundamentals of materials science and engineering*. *journal of chemical information and modeling*. Hoboken : John Wiley & Sons

Xue, B., Yin, S.-H., Yao, L. U. O., & Wu, W.-Y. (2011). Leaching kinetics of bastnaesite concentrate in HCl solution. *Transactions of Nonferrous Metals Society of China*, *21*(10), 2306–2310.

Yoon, H.-S., Kim, C.-J., Chung, K. W., Jeon, S., Park, I., Yoo, K., & Jha, M. K. (2015). The effect of grinding and roasting conditions on the selective leaching of Nd and Dy from NdFeB magnet scraps. *Metals*, *5*(3), 1306–1314.

Yoon, H.-S., Kim, C.-J., Chung, K. W., Lee, S.-J., Joe, A.-R., Shin, Y.-H., … Kim, J.-G. (2014). Leaching kinetics of neodymium in sulfuric acid from E-scrap of NdFeB

permanent magnet. *Korean Journal of Chemical Engineering*, *31*(4), 706–711.

Zhang, J., Zhao, B., & Schreiner, B. (2016). *Separation hydrometallurgy of rare earth elements*. Cham : Springer International Publishing.